Investigations of Magnetic Model Systems Using Coupled Cluster Based Approaches

by

Siyuan Wu

A thesis
presented to the University of Waterloo
in fulfillment of the
thesis requirement for the degree of
Master of Science
in
Chemistry

Waterloo, Ontario, Canada, 2017

© Siyuan Wu 2017

Author's Declaration

I hereby declare that I am the sole author of this thesis. This is a true copy of the thesis, including any required final revisions, as accepted by my examiners.

I understand that my thesis may be made electronically available to the public.

Abstract

Over the past decades, the quantum mechanical description of magnetic phenomena has been well developed. However, the first principle calculations of the physical properties of magnetic systems is still a challenge. One solution to the problem is to construct model magnetic Hamiltonians such that these Hamiltonians can well describe accurate energies of the low-lying magnetic states, starting from an *ab initio* Hamiltonian in a finite atomic orbital basis set.

In the first part of this work, the multireference equation of motion coupled cluster (MREOM-CC) approach including spin-orbit coupling is applied to model magnetic systems FArO, FArOF and FArFOH. All low-lying magnetic states are obtained subsequently from a compact diagonalization of the transformed Hamiltonian in the MREOM-CC scheme. The accuracy of MREOM is shown to be comparable to the well-established multireference Configuration Interaction with singles and doubles and the Davidson Q correction (MR-CISD+Q), but the MREOM approach is significantly more efficient for systems with a large number of electronic states.

In the second part, we discuss the details of the *effective Hamiltonian approach*, proposed in this work. The purpose of this approach is to obtain low-lying states for a Hamiltonian that consists of pairwise interactions between magnetic sites only. The approach includes two steps: the definition of an effective Hamiltonian that acts in a compact space of low-lying single-site states obtained from a mean-field calculation, and the diagonalization of the effective Hamiltonian. The last step still limits the size of systems that can be tackled. Some variants of the effective Hamiltonian approach are tested in benchmark applications to model magnetic systems. The results indicate that this approach is promising, and

finally we briefly discuss how this approach can be improved in the near future.

Acknowledgements

The two more years I stayed in the theoretical group must be the most unforgettable experience in my life. It is my great pleasure to say thanks to those people who offered help to me during this period.

First and foremost, I would like to express my deepest gratitude to my kind and respectable supervisor: Marcel Nooijen. Turning back time to Fall 2014, I took his advanced quantum chemistry course, which was a real challenge to me. When I asked him questions, he always put down his work intermediately, and patiently explained everything to me. He just opened the "gate" of quantum chemistry for me. During my master life with him, his enthusiasm towards science inspired me a lot. He also gave me a lot of lessons, such as "No pain, no gain", "Try to solve it by yourself first" and "Check everything carefully". These really helped develop my own thoughts towards research. Moreover, when I had personal issue, he was always there as a listener, and was willing to share his experience and give advice to me. He encouraged me a lot when I was frustrated, and was always supportive when I made any decision. Thank you, my life mentor!

I would like to thank Professor Germán Sciaini, who is one of my committee members, for offering much advice on my future career. Like you said, making a decision is never too hard, I should always follow my heart and do the things I am really interested in. Also, thanks for the coffee that you made when I dropped by your office each time.

I would like to thank my other committee members, Professors Roger Melko and Scott Hopkins for their comments on my thesis.

I would like to thank Prateek Goel, who acts as an elder brother to me. We had a lot

of beautiful conversations on both research and life. Sometimes, we made jokes on each other, and this really made the office life more active. In addition, thanks for sharing with me tricks on computational tools. Wish you all the best in Florida!

I would like to thank all the theoretical group members, especially Amanda Kwan, Neil Raymond and Dmitri Iouchtchenko, for their help and support.

I would like to thank my friends Wenjia Liu, Xudong Liu, Jingfei Yao, Weiqiang Fu and many others whom names I am forgetting here for those memorable moments here in Canada.

Last but not least, I would like to appreciate my parents, Jing Wu and Xiaoling Wu, for their endless love for me.

Dedication

This is dedicated to Ruiyi Zhao, the one who tolerates my shenanigans, the one I love.

Table of Contents

List of Tables

List of Figures

List of Abbreviations

CAS Complete Active Space 20

CASCI Complete Active Space Configuration Interaction 27

CASSCF Complete Active Space Self-Sonsistent Field 20

CI Configuration Interaction 15

DDCI difference dedicated Configuration Interaction 20

HDVV Heisenberg-Dirac-van Vleck 2

HF Hartree-Fock 13

IC-MRCI internally contracted Multireference Configuration Interaction 20

MRCI Multireference Configuration Interaction 3

MRCISD+Q Multireference Configuration Interaction with Singles and Doubles and the Davidson Correction 27

MREOM-CC Multireference Equation of Motion Coupled Cluster 3

SOC Spin-Orbit Coupling 3

SOMF Spin-Orbit Mean-Field 26

SRCC Single Reference Coupled Cluster 16

Chapter 1

Introduction

Magnetism is a phenomenon that has drawn the attention of humans during the development of human civilization. More than 2500 years ago, the first definite description of magnetism, that magnetite (Fe_3O_4) attracts iron, was described and has since grown into a major topic in the context of science [1].

As has been discussed in ref [2], the history of magnetism can be divided into seven ages: ancient(-1000-1500), early(1500-1820), electromagnetic(1820-1900), understanding(1900-1935), high frequency(1935-1960), applications(1960-1995) and spin electronics(1995-present). With the scope of magnetism expanding, applications of magnetism have crossed the ages, such as compass, horseshoe magnet, motors and magnetic recording devices [3].

In the past couple of decades, the development of molecular magnetism (that is, for the magnetic properties of materials based on molecules) has become an increasing interest for scientists [4]. In general, most chemical systems do not exhibit magnetism, because all electrons are paired in the populated low lying states. However, magnetism still occurs in

some systems varing from O_2 to metallic and ionic lattices [4, 5, 6].

The microscopic origin of magnetism is related to quantum mechanics. In general, one can explain most of the magnetic properties through the specific treatment of the electron spin [3]. Magnetic systems are characterized by the appearance of unpaired electrons. The wave functions of the states resulting from these electrons can be determined through the use of strongly correlated methods. However, the use of such methods with respect to an all-electron description cannot treat very large magnetic systems. As a result, a simplified model Hamiltonian that only considers the magnetic electrons is to be proposed to theoretically model their macroscopic properties and experimentally characterize them. To do so, one can employ the use of theoretical chemistry, which concerns the all-electron exact electronic Hamiltonian.

The use of theoretical chemistry has two main purposes [3]. The first important application is that one can deal with fragments of large size magnetic systems, such as large molecules, clusters or solids. The chemical features that are responsible for the magnetism can be obtained through the determination of the electronic structure of the low-lying states and their energies. Moreover, one can extract and derive model Hamiltonians from the energies and wave functions obtained using the exact electronic Hamiltonian.

A simple model spin Hamiltonian named Heisenberg-Dirac-van Vleck (HDVV) Hamiltonian is widely used with respect to the basis of pure spin functions [7, 8, 9]. The Hamiltonian expression for a multi-center system can be given by

$$\hat{H}_{HDVV} = -\sum_{i<j} J_{ij}(\hat{S}_i\hat{S}_j - \frac{n_i n_j}{4}\hat{I}) \tag{1.1}$$

where J_{ij} is the magnetic coupling parameter between two local magnetic units i and j, $\hat{S}_i$ and $\hat{S}_j$ are the spin operators, $\hat{I}$ is the identity operator, and n_i and n_j represent the number of unpaired electrons on centers i and j, respectively.

However, one may wonder from where the model Hamiltonian arises and how we may determine the Hamiltonian parameters like J_{ij}. If the model hamiltonian is known, one can possibly model experimental quantities like magnetic susceptibilities as a function of temperature. Conversely, experimental results can be used to extract model parameters. Unfortunately such results are not always unambiguous. In this work we are interested in calculating model magnetic Hamiltonian parameters from first-principles quantum chemistry calculations. This is a challenging task as one needs to calculate a number of electronic states that are very close in energy, and these systems are considered strongly correlated. The focus in this thesis is on calculating the low-lying states, and on extracting model Hamiltonians that upon diagonalization yield the same low-lying energies as the original ab initio calculations. However, our results will not be written in the form of a spin Hamiltonian as shown in Eq. (1.1). Let us now give a brief outline of the structure of the thesis.

Chapter 2 first provides an overview of some basic concepts in electronic structure theory and then discusses some single reference methods in quantum chemistry.

Chapter 3 reviews the application of strongly correlated methods on model magnetic systems. We first describe the underlying details of the newly developed Multireference Equation of Motion Coupled Cluster (MREOM-CC) approach [10, 11, 12] and the mean-field treatment of spin-orbit coupling (SOC) [13]. In the next step, two variants of MREOM methods are performed to benchmark the Multireference Configuration Interaction (MRCI)

calculation [14, 15] for the simple FArO model system. The results illustrate the robustness of MREOM. Finally, MREOM method is applied to magnetic systems that have up to four magnetic sites. The computational cost indicates the limitation of multireference methods with respect to large magnetic systems.

The last chapter is dedicated to investigating cost-effective approaches to obtain the low-lying energies for systems potentially consisting of many magnetic sites. The procedure involves the calculation of an effective Hamiltonian in the space of low-lying states, starting from a pair based hamiltonian in a much larger space. The effecitve Hamiltonian can include 3- and 4-body effects. The method is tailored to calculating states for systems that have a complicated structure. We will use similar magnetic model systems as in chapter 3, consisting of an Ar atom loosely bound to atoms like H, F, O, which have complicated multideterminantal ground state configurations. The results in chapter 4 are not yet complete, and in particular spin-orbit coupling is not yet considered. This chapter represents initial steps to the problem.

Chapter 2

Theoretical Background Theories

2.1 Elementary Concepts in Electronic Structure Theory

2.1.1 Hamiltonian with clamped nuclei

One of the central problems of *ab initio* electronic structure theory is to describe the motion of an electron in the field of certain nuclear point charges [16]. To do so, one main interest is to determine approximate solutions to the nonrelativistic time-independent Schrödinger equation

$$\hat{H}|\Psi\rangle = E|\Psi\rangle \tag{2.1}$$

where the Hamiltonian operator, wavefunction and energy for a system of electrons and nuclei are denoted as $\hat{H}, |\Psi\rangle$ and E, respectively. In general, the Hamiltonian for a system

of N electrons and M nuclei in atomic units is expressed as [16]

$$\hat{H} = -\sum_{i=1}^{N} \frac{1}{2}\nabla_i^2 - \sum_{A=1}^{M} \frac{1}{2M_A}\nabla_A^2 - \sum_{i=1}^{N}\sum_{A=1}^{M} \frac{Z_A}{r_{iA}} + \sum_{i=1}^{N}\sum_{i<j}^{N} \frac{1}{r_{ij}} + \sum_{A=1}^{M}\sum_{A<B}^{M} \frac{Z_A Z_B}{R_{AB}} \tag{2.2}$$

where indices A, B are labelled as nuclei, indices i, j are denoted as electrons. The first and second terms in the above equation represent the kinetic energy operator of electrons and nuclei, separately. The third term is the electron-nuclear coulomb attraction; the fourth and fifth terms indicate interelectronic repulsion and internuclear repulsion, respectively.

2.1.2 The Born-Oppenheimer Approximation

The Born-Oppenheimer approximation, which assumes that the motion of electrons and nuclei in a molecule can be separated, has been widely used in quantum chemistry and molecular physics. The success of this approximation is that the nuclei are much more massive than electrons; as a result, the electrons are considered to be moving in the field of fixed nuclei [17]. Within the approximation, one can neglect the kinetic energy of nuclei and also consider the internuclear repulsion to be a constant. In this case, the second term and last term of Eq. (2.2) can be neglected and the electronic Hamiltonian is given by

$$\hat{H} = -\sum_{i=1}^{N} \frac{1}{2}\nabla_i^2 - \sum_{i=1}^{N}\sum_{A=1}^{M} \frac{Z_A}{r_{iA}} + \sum_{i=1}^{N}\sum_{i<j}^{N} \frac{1}{r_{ij}} \tag{2.3}$$

2.1.3 The Antisymmetry Principle

The electronic Hamiltonian in Eq. (2.3) depends on the three spatial coordinates $\mathbf{r}$ of each electron. However, if we want to describe an electron completely, its spin coordinate ω also need to specified. In this formalism, an electron is described by three spatial coordinates and one spin coordinate coordinate. We express the collective four coordinates as $\mathbf{x}$,

$$\mathbf{x} = \{\mathbf{r}, \omega\} \tag{2.4}$$

The wave function for an N-electron system can be expressed as $\Phi(\mathbf{x}_1, \mathbf{x}_2, \cdots, \mathbf{x}_N)$. Since electrons are fermions, a many-electron wave function must be antisymmetric in terms of the interchange of the coordinate $\mathbf{x}$

$$\Phi(\mathbf{x}_1, \cdots, \mathbf{x}_i, \cdots, \mathbf{x}_j, \cdots, \mathbf{x}_N) = -\Phi(\mathbf{x}_1, \cdots, \mathbf{x}_j, \cdots, \mathbf{x}_i, \cdots, \mathbf{x}_N) \tag{2.5}$$

2.1.4 Orbitals and Slater Determinants

We define a spin orbital $\chi(\mathbf{x})$ as a wave function for an electron that describes both the spin and spatial distribution

$$\chi(\mathbf{x}) = \begin{cases} \psi(\mathbf{r})\alpha(\omega) \\ \quad \text{or} \\ \psi(\mathbf{r})\beta(\omega), \end{cases} \tag{2.6}$$

where $\psi(\mathbf{r})$ is spatial orbital, $\alpha(\omega)$ and $\beta(\omega)$ are two orthonormal functions that represent spin up ($\uparrow$) and spin down($\downarrow$), respectively. For each spatial orbital $\psi(\mathbf{r})$, spin up function

$\alpha(\omega)$ and spin down function $\beta(\omega)$ can be formed. As a result, given a set of K spatial orbitals $\{\psi_1(\mathbf{r}), \psi_2(\mathbf{r}), \cdots, \psi_K(\mathbf{r})\}$, one can obtain a orthonormal set of 2K spin orbitals $\{\chi_1(\mathbf{x}), \chi_2(\mathbf{x}), \cdots, \chi_{2K}(\mathbf{x})\}$

$$\left.\begin{aligned} \chi_{2i-1}(\mathbf{x}) &= \psi_i(\mathbf{r})\alpha(\omega) \\ \chi_{2i}(\mathbf{x}) &= \psi_i(\mathbf{r})\beta(\omega) \end{aligned}\right\} \quad i = 1, 2, \cdots, K \tag{2.7}$$

A Slater determinant that satisfies the antisymmetry principle is used to describe the wave function of N electrons occupying N spin orbitals $(\chi_1, \chi_2, \cdots, \chi_N)$

$$\Psi(\mathbf{x}_1, \mathbf{x}_2, \cdots, \mathbf{x}_N) = \frac{1}{\sqrt{N!}} \begin{vmatrix} \chi_1(\mathbf{x}_1) & \chi_2(\mathbf{x}_1) & \cdots & \chi_N(\mathbf{x}_1) \\ \chi_1(\mathbf{x}_2) & \chi_2(\mathbf{x}_2) & \cdots & \chi_N(\mathbf{x}_2) \\ \vdots & \vdots & \ddots & \vdots \\ \chi_1(\mathbf{x}_N) & \chi_2(\mathbf{x}_N) & \cdots & \chi_N(\mathbf{x}_N) \end{vmatrix}. \tag{2.8}$$

If one drops the normalization factor $\frac{1}{\sqrt{N!}}$ and only shows the diagonal elements of the determinant, a short-hand expression can be given by

$$\Psi(\mathbf{x}_1, \mathbf{x}_2, \cdots, \mathbf{x}_N) = |\chi_1(\mathbf{x}_1)\chi_2(\mathbf{x}_2)\cdots\chi_N(\mathbf{x}_N)\rangle \tag{2.9}$$

In a further way, if the electron labels are assigned to be in the order of $\mathbf{x}_1, \mathbf{x}_2, \cdots, \mathbf{x}_N$, the equation can be conveniently shortened to

$$\Psi(\mathbf{x}_1, \mathbf{x}_2, \cdots, \mathbf{x}_N) = |\chi_1\chi_2\cdots\chi_N\rangle \tag{2.10}$$

Then, the antisymmetry property of Slater determinant is expressed as

$$|\cdots\chi_i\cdots\chi_j\cdots\rangle = -|\cdots\chi_j\cdots\chi_i\cdots\rangle \tag{2.11}$$

A single Slater determinant is used as an approximation to the electronic wavefunction in Hartree-Fock theory. In more accurate theories, such as Configuration Interaction, a linear combination of Slater determinants is needed.

2.1.5 Second Quantization

First, we introduce an elegant way of treating many-electrons systems: second quantization. Second quantization is a technical tool to use the algebraic properties of certain operators to deal with the antisymmetry of the wave function.

The action of a creation operator $\hat{a}_i^\dagger$ operating on an arbitrary Slater determinant $|\chi_j\ldots\chi_k\rangle$ can be written as

$$\hat{a}_i^\dagger|\chi_j\ldots\chi_k\rangle = |\chi_i\chi_j\ldots\chi_k\rangle \tag{2.12}$$

Hence an electron is created in spin orbital χ_i by $\hat{a}_i^\dagger$.

The Slater determinant must follow the property of the antisymmetry principle. Consider

$$\hat{a}_i^\dagger\hat{a}_j^\dagger|\chi_k\ldots\chi_l\rangle = \hat{a}_i^\dagger|\chi_j\chi_k\ldots\chi_l\rangle \tag{2.13}$$

$$= |\chi_i\chi_j\chi_k\ldots\chi_l\rangle \tag{2.14}$$

On the other hand,

$$\hat{a}_j^\dagger \hat{a}_i^\dagger |\chi_k \dots \chi_l\rangle = \hat{a}_j^\dagger |\chi_i \chi_k \dots \chi_l\rangle \tag{2.15}$$

$$= |\chi_j \chi_i \chi_k \dots \chi_l\rangle \tag{2.16}$$

$$= -|\chi_i \chi_j \chi_k \dots \chi_l\rangle \tag{2.17}$$

Adding Eq. (2.14) and Eq. (2.17) we obtain

$$\hat{a}_i^\dagger \hat{a}_j^\dagger |\chi_k \dots \chi_l\rangle + \hat{a}_j^\dagger \hat{a}_i^\dagger |\chi_k \dots \chi_l\rangle = (\hat{a}_i^\dagger \hat{a}_j^\dagger + \hat{a}_j^\dagger \hat{a}_i^\dagger)|\chi_k \dots \chi_l\rangle \tag{2.18}$$

$$= 0 \tag{2.19}$$

Since $|\chi_j \dots \chi_k\rangle$ is arbitrary, the anticommutator of two creation operators $\hat{a}_i^\dagger$, $\hat{a}_j^\dagger$ is given by

$$\left\{\hat{a}_i^\dagger, \hat{a}_j^\dagger\right\} = \hat{a}_i^\dagger \hat{a}_j^\dagger + \hat{a}_j^\dagger \hat{a}_i^\dagger = 0 \tag{2.20}$$

Consequently, the antisymmetry property of the Slater determinant is encoded through the anticommutation relation.

Next, we will introduce the annihilation operator, which is defined as the adjoint of the creation operator $\hat{a}_i^\dagger$ (i.e., $((\hat{a}_i^\dagger)^\dagger = \hat{a}_i)$). Analogously to Eq. (2.12), $\hat{a}_i$ is defined as removing the electron from an occupied spin orbital χ_i,

$$\hat{a}_i |\chi_i \chi_j \dots \chi_k\rangle = |\chi_j \dots \chi_k\rangle. \tag{2.21}$$

If the spin orbital is not immediately to the left, a number of transpositions is required to interchange the columns of the determinant, e.g.,

$$\hat{a}_i|\chi_j\chi_i\cdots\chi_k\rangle = -\hat{a}_i|\chi_i\chi_j\cdots\chi_k\rangle = -|\chi_j\cdots\chi_k\rangle \tag{2.22}$$

There are two more anticommutators reflecting the antisymmetry principle.

$$\{\hat{a}_i, \hat{a}_j\} = \hat{a}_i\hat{a}_j + \hat{a}_j\hat{a}_i = 0 \tag{2.23}$$

$$\left\{\hat{a}_i^\dagger, \hat{a}_j\right\} = \hat{a}_i^\dagger\hat{a}_j + \hat{a}_j\hat{a}_i^\dagger = \delta_{ij} = \begin{cases} 1, & i = j \\ 0, & i \neq j \end{cases} \tag{2.24}$$

To obtain the second-quantized representation of the Slater determinant, we introduce the vacuum state denoted by $|\text{vac}\rangle$. That is, it contains no electron. In general,

$$\hat{a}_i^\dagger\hat{a}_j^\dagger\ldots\hat{a}_k^\dagger|\text{vac}\rangle = |\chi_i\chi_j\ldots\chi_k\rangle \tag{2.25}$$

$$\langle\text{vac}|\hat{a}_k\ldots\hat{a}_j\hat{a}_i = \langle\chi_k\ldots\chi_j\chi_i| \tag{2.26}$$

2.1.6 Normal Ordering and Wick's Theorem

In quantum chemistry, there are a number of approaches in which one wants to evaluate the matrix element $\langle\text{vac}|\widehat{A}\widehat{B}\widehat{C}\cdots|\text{vac}\rangle$, where $\widehat{A}, \widehat{B}, \widehat{C}, \cdots$ are expressed using strings of second-quantized creation and annihilation operators. Then the so-called *normal-ordered product* of such operators is defined as the rearranged product of operators such that all creation operators are to the left of all annihilation operators in the product. Moreover, a minus sign

arises from each of the permutations of adjacent operators producing the rearrangement product. For example, $\left\{a_i^\dagger a_j\right\} = a_i^\dagger a_j$, $\left\{a_j a_i^\dagger\right\} = -a_i^\dagger a_j$ are the rearranged normal-ordered products, where the braces indicate the normal-ordered action on the vacuum state. The vacuum expectation value of a normal-ordered product is zero, which can be expressed as

$$\langle \text{vac}| \left\{\widehat{A}\widehat{B}\widehat{C}\cdots\right\} |\text{vac}\rangle = 0 \tag{2.27}$$

Wick's theorem is used extensively in the evaluation of the expectation values of operator strings. In order to formulate this, we define the *contraction* of a pair of second-quantized operators $\widehat{A}$, $\widehat{B}$ [18] as

$$\overbracket{\widehat{A}\widehat{B}} = \widehat{A}\widehat{B} - \{\widehat{A}\widehat{B}\}, \tag{2.28}$$

Here, there are four possibilities to be considered:

$$\overbracket{\hat{a}_i^\dagger \hat{a}_j^\dagger} = \hat{a}_i^\dagger \hat{a}_j^\dagger - \{\hat{a}_i^\dagger \hat{a}_j^\dagger\} = \hat{a}_i^\dagger \hat{a}_j^\dagger - \hat{a}_i^\dagger \hat{a}_j^\dagger = 0, \tag{2.29}$$

$$\overbracket{\hat{a}_i^\dagger \hat{a}_j} = \hat{a}_i^\dagger \hat{a}_j - \{\hat{a}_i^\dagger \hat{a}_j\} = \hat{a}_i^\dagger \hat{a}_j - \hat{a}_i^\dagger \hat{a}_j = 0, \tag{2.30}$$

$$\overbracket{\hat{a}_i \hat{a}_j} = \hat{a}_i \hat{a}_j - \{\hat{a}_i \hat{a}_j\} = \hat{a}_i \hat{a}_j - \hat{a}_i \hat{a}_j = 0, \tag{2.31}$$

$$\overbracket{\hat{a}_j \hat{a}_i^\dagger} = \hat{a}_j \hat{a}_i^\dagger - \{\hat{a}_j \hat{a}_i^\dagger\} = \hat{a}_j \hat{a}_i^\dagger - \left(-\hat{a}_i^\dagger \hat{a}_j\right) = \left\{\hat{a}_i^\dagger, \hat{a}_j\right\} = \delta_{ij}. \tag{2.32}$$

Therefore, the contraction of two creation or annihilation operators is equal to zero or one. A normal-ordered product with contractions can be given by

$$\{\widehat{A}\widehat{B}\widehat{C}\cdots\overbracket{\widehat{P}\cdots\overbracket{\widehat{Q}\cdots\overbracket{\widehat{R}\cdots\widehat{S}}}}\cdots\} = (-1)^\delta \overbracket{\widehat{P}\widehat{R}}\overbracket{\widehat{Q}\widehat{S}}\cdots\{\widehat{A}\widehat{B}\widehat{C}\cdots\}, \tag{2.33}$$

where δ is the number of transpositions to bring contracted operators in adjacent positions. In addition, the time-independent Wick's theorem [19] states: a string of creation and annihilation operators can be rewritten as their normal-ordered product plus the sum of normal-ordered products with all possible contractions

$$\begin{aligned}
\widehat{A}\widehat{B}\widehat{C}\widehat{D}\cdots &= \{\widehat{A}\widehat{B}\widehat{C}\widehat{D}\cdots\} + \underbrace{\left[\{\overbrace{\widehat{A}\widehat{B}}\widehat{C}\widehat{D}\cdots\} + \{\widehat{A}\overbrace{\widehat{B}\widehat{C}}\widehat{D}\cdots\} + \{\widehat{A}\overbrace{\widehat{B}\widehat{C}\widehat{D}}\cdots\} + \{\widehat{A}\widehat{B}\overbrace{\widehat{C}\widehat{D}}\cdots\} + \ldots\right]}_{\text{One pair contractions}} \\
&+ \underbrace{\left[\{\overbrace{\widehat{A}\widehat{B}}\overbrace{\widehat{C}\widehat{D}}\cdots\} + \{\overbrace{\widehat{A}\overbrace{\widehat{B}\widehat{C}}\widehat{D}}\cdots\} + \ldots\right]}_{\text{Two pairs contractions}} + \ldots + \sum_{\substack{\text{fully}\\ \text{contracted}}} \{\overbrace{\widehat{A}\widehat{B}\widehat{C}\widehat{D}\cdots}\} \\
&= \{\widehat{A}\widehat{B}\widehat{C}\widehat{D}\cdots\} + \sum_{\substack{\text{all possible}\\ \text{contractions}}} \{\overbrace{\widehat{A}\widehat{B}\widehat{C}\widehat{D}\cdots}\}
\end{aligned} \tag{2.34}$$

2.2 Single Reference Approaches

2.2.1 The Hartree-Fock Method

The Hartree-Fock (HF) approximation plays a significant role in approximately solving the electronic Schrödinger equation, and it assumes that a single Slater determinant can be used to approximate the ground state of an N-electron system.

$$|\Psi_0\rangle = |\chi_1\chi_2\cdots\chi_a\chi_b\cdots\chi_N\rangle \tag{2.35}$$

The spin orbitals in $|\Psi_0\rangle$ are optimized such that the energy is minimized

$$E_0 = \langle \Psi_0 | \hat{H} | \Psi_0 \rangle \tag{2.36}$$

where $\hat{H}$ is the electronic Hamiltonian.

Even though the HF wave function is the simplest form of an antisymmetric wave function, the accuracy of the simplest approximation is surprisingly good. The HF energy can capture more than 99% of the total energy. Unfortunately, the remaining energy is extremely important in the context of chemistry. For example, the Hartree-Fock energy of water with respect to the cc-pV6Z basis set is -76.067401 Hartree [20]. 1% of this is about 0.76 Hartree or 2000 kJ/mol! In addition, the Hartree-Fock wavefunctions account for around 70% of the dissociation energy of water, as has been discussed in [21]. As a result, one needs to solve the Schrödinger equation more accurately.

2.2.2 Excited Determinant and Configuration Interaction

The Hartree-Fock procedure can produce a set of N occupied spin orbitals $\{\chi_i\}$. The number of single determinants formed from an N-electron system and 2K spin orbitals is

$$\binom{2K}{N} = \frac{(2K)!}{N!(2K-N)!} \tag{2.37}$$

One of these single determinants can describe the Hartree-Fock ground state, while other single determinants are basis functions that can be used to improve accuracy of HF method, or for the description of singly, doubly, triply, quadruply, ... , N-tuply excited states.

For example, in a so-called single excited determinant, an electron is excited from an occupied spin orbital χ_a in Hartree-Fock ground state, to a virtual spin orbital χ_r

$$|\Psi_a^r\rangle = |\chi_1\chi_2\cdots\cancel{\chi_a}\chi_r\chi_b\cdots\chi_N\rangle \tag{2.38}$$

A doubly excited determinant corresponds to a pair of electrons that have been excited from two occupied spin orbitals χ_a and χ_b to two virtual spin orbitals χ_r and χ_s

$$|\Psi_{ab}^{rs}\rangle = |\chi_1\chi_2\cdots\cancel{\chi_a}\chi_r\cancel{\chi_b}\chi_s\cdots\chi_N\rangle \tag{2.39}$$

The full Configuration Interaction (CI) wave function can be expressed by a linear combination of all the possible determinants

$$\begin{aligned}|\Phi_{\mathrm{FCI}}\rangle &= c_0\,|\Psi_0\rangle + \sum_a^N\sum_r^{2K} c_a^r\,|\Psi_a^r\rangle + \sum_{a<b}^N\sum_{r<s}^{2K} c_{ab}^{rs}\,|\Psi_{ab}^{rs}\rangle + \sum_{a<b<c}^N\sum_{r<s<t}^{2K} c_{abc}^{rst}\,|\Psi_{abc}^{rst}\rangle + \cdots \\ &= \sum_\mu c_\mu\,|\Psi_\mu\rangle\,,\end{aligned} \tag{2.40}$$

and these coefficients are obtained by minimizing the energy

$$E = \frac{\langle\Phi_{\mathrm{FCI}}|\hat{H}|\Phi_{\mathrm{FCI}}\rangle}{\langle\Phi_{\mathrm{FCI}}|\Phi_{\mathrm{FCI}}\rangle} \tag{2.41}$$

When solving for the energy, the full CI Hamiltonian matrix will lead to the eigenvalue problem

$$\sum_\mu \langle\Psi_\lambda|\hat{H}|\Psi_\mu\rangle c_\mu = \sum_\mu E\delta_{\mu\lambda}c_\mu = Ec_\lambda \tag{2.42}$$

which can be rewritten as

$$\mathbf{Hc} = E\mathbf{c} \tag{2.43}$$

The full CI problem describes the exact solution of the Schrödinger equation in a given basis set. Unfortunately, it is very expensive to compute for infinite basis sets. Therefore, the goal of quantum chemistry is to define suitable approximations.

2.2.3 Single Reference Coupled Cluster Theory

The Single Reference Coupled Cluster (SRCC) treatment is widely used in quantum chemistry. It works very well if the HF wave function is a good starting point.
In SRCC theory [22, 23], the ground state wave function is written as an exponential ansatz

$$|\psi\rangle = e^{\hat{T}}|\Psi_0\rangle \tag{2.44}$$

$$= (1 + \hat{T} + \frac{\hat{T}^2}{2!} + \frac{\hat{T}^3}{3!} + \cdots)|\Psi_0\rangle \tag{2.45}$$

where $\hat{T}$ is the cluster operator and $|\Psi_0\rangle$ is the Hartree-Fock ground state. The cluster operator $\hat{T}$ in SRCC theory is defined as

$$\hat{T} = \hat{T}_1 + \hat{T}_2 + \cdots \tag{2.46}$$

$$= \sum_i \sum_a t_i^a \hat{a}^\dagger \hat{i} + \frac{1}{4} \sum_{i,j} \sum_{a,b} t_{ij}^{ab} \hat{a}^\dagger \hat{b}^\dagger \hat{j} \hat{i} + \cdots \tag{2.47}$$

In the above formula, the indices i, j refer to occupied spin orbitals in the reference function $|\Psi_0\rangle$, while a, b stand for the unoccupied orbitals. $\hat{a}^\dagger, \hat{b}^\dagger$ denote the creation operators,

and $\hat{i}, \hat{j}$ indicate the annihilation operators. The coefficients t_i^a, t_{ij}^{ab} are called the cluster amplitudes.

The non-relativistic time-independent Schrödinger equation in SRCC theory can be written as

$$\hat{H}e^{\hat{T}}|\Psi_0\rangle = Ee^{\hat{T}}|\Psi_0\rangle \tag{2.48}$$

$$e^{-\hat{T}}\hat{H}e^{\hat{T}}|\Psi_0\rangle = Ee^{-\hat{T}}e^{\hat{T}}|\Psi_0\rangle \tag{2.49}$$

$$e^{-\hat{T}}\hat{H}e^{\hat{T}}|\Psi_0\rangle = E|\Psi_0\rangle \tag{2.50}$$

The SRCC cluster amplitudes and energy can be obtained by projecting against the excited state determinant ($\langle\Psi^*|$) and the ground state determinant on Eq. (2.50), respectively

$$\langle\Psi^*|e^{-\hat{T}}\hat{H}e^{\hat{T}}|\Psi_0\rangle = 0 \tag{2.51}$$

$$\langle\Psi_0|e^{-\hat{T}}\hat{H}e^{\hat{T}}|\Psi_0\rangle = E \tag{2.52}$$

The transformed Hamiltonian in SRCC theory can be denoted as $\hat{\bar{H}}$

$$\hat{\bar{H}} = e^{-\hat{T}}\hat{H}e^{\hat{T}} \tag{2.53}$$

$$= \hat{H} + [\hat{H}, \hat{T}] + \frac{1}{2!}[[\hat{H}, \hat{T}], \hat{T}] + \cdots \tag{2.54}$$

The main advantage of Coupled Cluster theory is that the choice of exponential ansatz guarantees the size-consistency of the solution.

The original Schrödinger equation is given by

$$\hat{H}|\Psi\rangle = E|\Psi\rangle \tag{2.55}$$

We can transform Eq. (2.55) to obtain the general transformed Hamiltonian.

$$\begin{aligned} \hat{H}UU^{-1}|\Psi\rangle &= E|\Psi\rangle & (2.56)\\ U^{-1}\hat{H}UU^{-1}|\Psi\rangle &= EU^{-1}|\Psi\rangle & (2.57)\\ \hat{\bar{H}}U^{-1}|\Psi\rangle &= EU^{-1}|\Psi\rangle & (2.58)\\ \hat{\bar{H}}|\phi\rangle &= E|\phi\rangle & (2.59) \end{aligned}$$

where the transformed Hamiltonian with respect to an arbitrary operator U is written as

$$\hat{\bar{H}} = U^{-1}\hat{H}U \tag{2.60}$$

It is seen that the original Hamiltonian and transformed Hamiltonian have same eigenvalues, but yield different eigenstates $|\phi\rangle = U^{-1}|\Psi\rangle$.

In the remaining chapters, the concept of a similarity transformation will be used repeatedly. By choosing the operator U in a suitable fashion, the eigenfunction $|\phi\rangle$ of the transformed Hamiltonian can be greatly simplified. CC theory is an example of such a theory, and the ground state of the transformed Hamiltonian is the Hartree-Fock determinant. All the complexity of the problem is transfered to the operator U.

Chapter 3

Multireference Equation of Motion Coupled Cluster Benchmark Study of Magnetic Model Systems[1]

3.1 Introduction

Human knowledge of magnetic phenomena has a very long history, going back to ancient times [2]. Today, the quantum mechanical description of magnetic phenomena is well understood, but the first principle calculations of magnetic properties is still a challenge [3]. A convenient approach to the problem is the construction of a model magnetic Hamiltonian [24, 25], and the extraction of the parameters that enter the Hamiltonian from first principle quantum chemistry approaches (e.g., see refs. [26, 27]). These approaches are well

[1]The contents of this chapter have been submitted for publication in *J. Chem. Theory Comput.*

established, and have been reviewed, for example, in refs. [3, 28]. The choice of quantum chemistry approach is delicate. Broken symmetry density functional theory (DFT) [29, 30] has been used extensively in the past [31, 32, 33, 34, 35], and has the virtue that the approach is efficient, but it also heavily relies on the assumed validity of the model Hamiltonian, and further underlying assumptions. A more satisfactory approach would be based on accurate wave function techniques that are suitable for strongly correlated systems. A method that has created significant interest is the difference dedicated Configuration Interaction (DDCI) approach [36, 37, 38, 39]. However, this method is expensive, using a large CI expansion, and in particular uses a threshold to screen configurations. Therefore, the method is somewhat delicate to apply. A clear alternative would be the internally contracted Multireference Configuration Interaction (IC-MRCI) approach [14, 15]. However, this approach can also be expensive and it requires a balanced treatment of many low-lying electronic states.

In this work we consider the applicability of the newly developed multireference equation of motion coupled cluster (MREOM-CC) approach [10, 11, 12]. This methodology has clear advantages for magnetic systems. In the context of MREOM, one starts with a state-averaged complete active space self-consistent field (CASSCF) calculation [40] and in the case of magnetic systems this CASSCF calculation can simply comprise the high-spin states in the system, which can usually be described using a small number of configurations. In addition, the choice of active orbitals is elementary for magnetic systems. In subsequent steps, a number of similarity transformations of the Hamiltonian are obtained, solving for the amplitudes along the way. To calculate the similarity transforms, one only requires the one and two-body reduced density matrices corresponding to the state-averaged complete

active space (CAS). In the final step of MREOM, the transformed Hamiltonian is diagonalized over CAS, 1h and 1p configurations. The dimension of the final diagonalization space is very compact and one can obtain all low-lying magnetic states of interest in this final diagonalization step, in particular also low-spin states. Because the final diagonalization space is small, it is feasible to calculate systems with a sizeable number of magnetic atoms. Moreover, the MREOM implementation in ORCA [41, 42, 43] provides a treatment of spin-orbit coupling (SOC) [13].

The purpose of this paper is to determine the accuracy of MREOM including SOC for magnetic systems. To do this, we design artificial magnetic systems that are fairly easy to compute, and we can compare MREOM results to benchmark MRCI+Q, both including a treatment of SOC. The artificial magnetic systems consist of open-shell atoms like F, O or H and a closed-shell Ar atom. Magnetic atoms are interacting with each other, while Ar atom acts like a bridge in the magnetic system and accounts for so-called super-exchange [44, 45, 46]. It will be demonstrated that SOC_MREOM results follow SOC_MRCI+Q results quite closely, while in addition the MREOM results are size-consistent for all practical purposes. Therefore, one can establish the geometrical dependence of the magnetic interactions. This paper is organized as follows. In section 3.2, we discuss the underlying theory of MREOM and the mean-field treatment of SOC. In section 3.3, computational details regarding some variants of MREOM, and the details concerning the MRCI calculation in Molpro [47] are discussed. In section 3.4, we provide in depth comparisons for the simple FArO model system, and we discuss a modification to the default spin-orbit mean-field method in ORCA to maintain size-consistency. MREOM is then applied to magnetic systems that have up to four magnetic sites to establish the promise of the method.

3.2 Theory

The MREOM-CC approach [10, 11, 12] provides a convenient way to calculate a large number of electronic excited states using an efficient transform and diagonalize strategy. The starting point of MREOM calculation is a state-averaged CASSCF calculation, where all states of interest are considered to be qualitatively well described by linear combination of electronic configurations which comprise the CAS. Let us denote i', j', k', l' as inactive core orbitals, w, x, y, z, as active orbitals, i, j, k, l as occupied orbitals, which can be either inactive or active, a, b, c, d, as virtual orbitals, p, q, r, s, as general orbitals. The key idea of MREOM methodology is that a sequence of many-body similarity transformations are applied to the second-quantized Hamiltonian. In general, many body transformations with respect to Kutzelnigg-Mukherjee normal ordering [48, 49, 50], can be expressed as follow:

$$\begin{aligned}
\hat{G} &= \left\{e^{\hat{Y}}\right\}^{-1} \hat{H}\left\{e^{\hat{Y}}\right\} \rightarrow \left\{e^{\hat{Y}}\right\} \hat{G} = \hat{H}\left\{e^{\hat{Y}}\right\} \rightarrow, \\
\hat{G} &= (\hat{H}\left\{e^{\hat{Y}}\right\})_{Connected} - (\left\{e^{\hat{Y}} - 1\right\} \hat{G})_{Connected} = ... \\
&= g_0 + g_r^p \{p^\dagger r\} + \frac{1}{4} g_{rs}^{pq} \{p^\dagger r q^\dagger s\} + \cdots .
\end{aligned} \tag{3.1}$$

A key observation is that such a transformed Hamiltonian is explicitly a connected operator if $\hat{Y}$ is connected, which is the case in MREOM.

In this work, we will describe a sequence of transformations which has been implemented in the ORCA package, and which in full is referred to as the MR-EOM-T|T†|SXD|U method. We will consider the implementation of operators $\hat{T}, \hat{S}, \hat{X}, \hat{D}, \hat{U}$ in terms of similarity transformations. Below, we use the Einstein summation convention meaning that

repeated indices are always summed over.

The excitation operator $\hat{T}$ expressed in terms of the single and double spin-free generators of the unitary group $\hat{E}^q_p$ and $\hat{E}^{rs}_{pq}$ is given by

$$\hat{T} = \hat{T}_1 + \hat{T}_2 = t^i_a \hat{E}^a_i + \frac{1}{2} t^{ij}_{ab} \hat{E}^{ab}_{ij}, \tag{3.2}$$

where t^i_a and t^{ij}_{ab} are single and double excitation amplitudes, respectively.

The Hamiltonian $\hat{H}$ is expressed in the usual second-quantized form, and the first transformation in MREOM is obtained as

$$\begin{aligned} \hat{\bar{H}} &= e^{-\hat{T}} \hat{H} e^{\hat{T}} \\ &= \bar{h}_0 + \bar{h}^p_q \left\{ \hat{E}^q_p \right\} + \bar{h}^{pq}_{rs} \left\{ \hat{E}^{rs}_{pq} \right\} + \bar{h}^{pqr}_{stu} \left\{ \hat{E}^{stu}_{pqr} \right\} + \cdots , \end{aligned} \tag{3.3}$$

noting that $e^{\hat{T}}$ is already in normal-ordered form.

The t-amplitudes are solved from [12, 51]

$$\sum_k \omega_k \langle R_k | E^i_a \hat{\bar{H}} | R_k \rangle = 0, \tag{3.4}$$

$$\bar{h}^{ab}_{ij} = \bar{h}^{ab}_{ix} = \bar{h}^{ab}_{xy} = 0, \tag{3.5}$$

where $|R_k\rangle$ refers to states obtained from the state-averaged CASSCF and ω_k is the corresponding state weight.

The second transformation in the MR-EOM-T|T†|SXD|U scheme [42] is written as

$$\begin{aligned}\hat{\tilde{\mathcal{H}}} &= e^{\hat{T}^\dagger}\hat{\bar{H}}_2 e^{-\hat{T}^\dagger} \\ &= \tilde{h}_0 + \tilde{h}^q_p\left\{\hat{E}^p_q\right\} + \tilde{h}^{rs}_{pq}\left\{\hat{E}^{pq}_{rs}\right\} + \tilde{h}^{stu}_{pqr}\left\{\hat{E}^{pqr}_{stu}\right\} + \cdots,\end{aligned} \tag{3.6}$$

in which $\hat{\bar{H}}_2$ is the similarity transformed Hamiltonian in Eq. (3.3), truncated up to two-body operators. The de-excitation operator $\hat{T}^\dagger$ is defined as

$$\hat{T}^\dagger = t^a_i \hat{E}^i_a + \frac{1}{2} t^{ab}_{ij}\hat{E}^{ij}_{ab}, \tag{3.7}$$

and the de-excitation amplitudes are assumed to be the same as the excitation amplitudes

$$t^a_i \approx t^i_a, \tag{3.8}$$

$$t^{ab}_{ij} \approx t^{ij}_{ab}. \tag{3.9}$$

The similarity transformation of Eq. (3.6) is performed to make the Hamiltonian $\hat{\tilde{\mathcal{H}}}$ approximately Hermitian.

The third transformation takes the form

$$\bar{F} = \left\{e^{\hat{S}_2+\hat{X}+\hat{D}}\right\}^{-1}\hat{\tilde{\mathcal{H}}}_2\left\{e^{\hat{S}_2+\hat{X}+\hat{D}}\right\}, \tag{3.10}$$

in which $\hat{\tilde{\mathcal{H}}}_2$ include the zero-, one- and two-body elements of $\hat{\tilde{\mathcal{H}}}$ in Eq. (3.6). Here the

$\hat{S}_2, \hat{X}$ and $\hat{D}$ operators are defined as

$$\hat{S}_2 = s^{ax}_{i'j'} \hat{E}^{i'j'}_{ax}, \tag{3.11}$$

$$\hat{X} = \hat{X}_2 = x^{ay}_{xj'} \hat{E}^{xj'}_{ay}, \tag{3.12}$$

$$\hat{D} = \hat{D}_2 = d^{ay}_{i'x} \hat{E}^{i'x}_{ay}. \tag{3.13}$$

The SXD-amplitudes are solved from

$$f^{ax}_{i'j'} = f^{ay}_{xj'} = f^{ay}_{i'x} = 0. \tag{3.14}$$

In all above expressions, we only retain terms that are at most quadratic in the cluster amplitudes [11].

The final similarity transformation of the MR-EOM-T|T†|SXD|U approach is given by

$$\begin{aligned} \hat{G} &= e^{-\hat{U}} \hat{F}_2 e^{\hat{U}} \\ &= g_0 + g^p_q \left\{ \hat{E}^q_p \right\} + g^{pq}_{rs} \left\{ \hat{E}^{rs}_{pq} \right\} + g^{pqr}_{stu} \left\{ \hat{E}^{stu}_{pqr} \right\} + \cdots, \end{aligned} \tag{3.15}$$

where $\hat{F}_2$ indicates that $\hat{F}$ in Eq. (3.10) has been truncated up to two-body operators. The operator $\hat{U}$ is defined as

$$\hat{U} = \hat{U}_2 = \frac{1}{2} u^{xy}_{i'j'} \hat{E}^{i'j'}_{xy}. \tag{3.16}$$

The U-amplitudes are solved from

$$g^{xy}_{i'j'} = 0. \tag{3.17}$$

Once again, we discard terms that are more than quadratic in the amplitudes. All MREOM amplitudes equations are expressed in terms of spatial state-averaged one-particle reduced density matrices, and the state-averaged two-body cumulant. The detailed equations have been derived using computer algebra, and a code generator is used to develop the computer code in ORCA, written in the C++ language [41, 42].

The inclusion of SOC has been discussed in previous studies [13, 52, 53]. A good starting point to introduce the SOC effect is that a number of I electronic states

$$|\Psi_I^{SS}\rangle = \sum_\mu C_{\mu I} |\Phi_\mu^{SS}\rangle \tag{3.18}$$

are obtained following the diagonalization of the similarity transformed Hamiltonian [42, 53]. For the inclusion of SOC effects, the functions $|\Psi_I^{SM}\rangle$ with spin projection number $M = -S, \cdots, S$ can be generated by the repeated application of spin shift operators on the states $|\Psi_I^{SS}\rangle$. The energies of basis states $|\Psi_I^{SM}\rangle$ treated by the quasi-degenerate perturbation theory can be obtained by

$$\langle \Psi_I^{SM} | \hat{G} + \hat{H}_{SOMF} | \Psi_J^{S'M'} \rangle = \delta_{IJ}\delta_{SS'}\delta_{MM'} E_I^{(S)} + \langle \Psi_I^{SM} | \hat{H}_{SOMF} | \Psi_J^{S'M'} \rangle, \tag{3.19}$$

where the spin-orbit mean-filed (SOMF) operator is described in refs. [13, 54] and the calculation of the SOMF matrix elements is given in ref. [53]. In this formulation, it is crucial that the MREOM Hamiltonian $\hat{G}$ commutes with the spin operators. In addition, we use the bare $\hat{H}_{SOMF}$ rather than a transformed SOC operator. This is an approximation that has been shown to work fairly well for atoms [55].

3.3 Computational Details

The main strategy of MREOM methods for studying magnetic systems is that many electronic excited states can be obtained, while the preceding state-averaged CASSCF calculation is performed for only a few high-spin states. The amplitudes in MREOM are solved using state-averaged density matrices from the CASSCF calculation. As shown in Table 3.1, two variations of MREOM including the definition of final MRCI diagonalization space are discussed.

In this work, we employ both ORCA and Molpro quantum chemistry packages. The complete active space configuration interaction (CASCI) or CASSCF and MRCISD+Q [14, 15, 56, 57] approaches are performed to study the effect of dynamic correlation using the Molpro package. Moreover, two MREOM approaches listed in Table 3.1 are performed in ORCA to test the efficiency and the accuracy of the transform and diagonalize strategy.

Method	Short name	Transformation(s)	Diagonalization space
MR-EOM-T|T†|SXD|U	MREOM	$\hat{T}_1 + \hat{T}_2 \| \hat{T}_1^\dagger + \hat{T}_2^\dagger \| \hat{S}_2 + \hat{X} + \hat{D} \| \hat{U}$	CAS, 1p,1h
MR-EOM-T|T†|SXD-ph	MREOM_1p1h	$\hat{T}_1 + \hat{T}_2 \| \hat{T}_1^\dagger + \hat{T}_2^\dagger \| \hat{S}_2 + \hat{X} + \hat{D}$	CAS, 1p,1h, 2h, 1p1h

Table 3.1: The characteristics of the two MREOM approaches.

All calculation that include SOC are denoted as SOC_CASCI, SOC_MRCISD+Q, SOC_MREOM and SOC_MREOM_1p1h, and are performed to understand the effect of SOC on magnetic systems. The default SOC approach in ORCA is defined as SOMF(1X), which has been discussed in ref. [13]. In this default approach, there is a tight threshold to include only states that are nearly degenerate with the ground state. This is not a good

strategy for systems studied in this work (as will be shown later). Instead we use a modified SOMF(1X) approach denoted as m_SOMF(1X) in which the state-averaged density passed to the SOC program is obtained over *all states*. It is also important to note here that a full SOC_MRCISD+Q calculation in Molpro requires a lot of memory. Therefore, a lower level of accuracy approach is used in the Molpro package. The wavefunctions passed to the spin-orbit program are generated by the MRCI with singles only, while the diagonal elements are replaced by precomputed MRCISD+Q energies.

All calculations were performed using the cc-pVDZ basis set [58, 59].

3.4 Results

3.4.1 Analysis of Results for the FArO System

Let us first introduce the FArO artificial magnetic system. The geometric structure of the system is given in Figure 3.1. To design a representative magnetic system, the distance

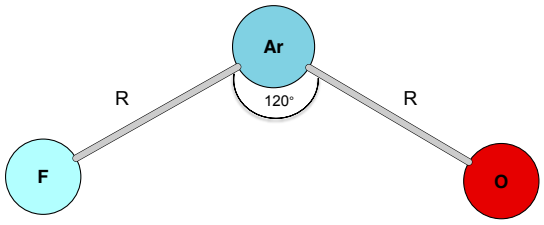

Figure 3.1: The geometric structure of the FArO system. $R = r(Ar - F) = r(Ar - O)$, bond angle is 120°.

between F, O and Ar is fairly large. Hence, the system essentially consists of the magnetic atoms F and O interacting with a spacer, while the atomic degeneracy is further lifted through interaction of F and O. In reality, this system is highly unstable as the distant open-shell atoms would react to molecules that are then weakly bounded to argon atom. In our calculation, we constrain the geometries such that the open-shell identities of the atoms in the cluster is preserved. In this section, we first give a brief qualitative picture and analysis of such magnetic systems. In doing so, we have decided to look at the effect of the Argon atom, spin-orbit coupling, dynamical correlation and magnetic coupling. In addition, we report our analysis on testing the accuracy of the multireference methods performed in this work. Finally, we present some results on the analysis of FArO at smaller distances.

3.4.1.1 Consideration of the Argon Atom and Spin-orbit Coupling

We start from a CASCI using the Molpro package to illustrate the effect of spin-orbit coupling and inclusion of the Ar atom on the statistical-mechanical properties analysis of the low-lying states of magnetic molecules. At first, CASCI and SOC_CASCI calculations have been performed for FArO and FXO at bond length R = 2.9 Å. In FXO, the Ar atom is replaced by auxiliary center such that F and O atoms are at the same positions as in FArO. Below, we more conveniently denote FXO as FO. To illustrate the results of the calculation in a convenient fashion, we draw a curve of excitation energy versus state number referred to as an excitation energy plot, and we also provide the heat capacity as a function of temperature. The heat capacity is obtained from a sum over states expression, that includes all low-lying magnetic states. Given each energy level E_n and temperature

T, we define

$$Z = \sum_{n=0} e^{\frac{-(E_n - E_0)}{k_B T}} \tag{3.20}$$

$$P_n = \frac{1}{Z} e^{\frac{-(E_n - E_0)}{k_B T}} \tag{3.21}$$

$$U = \sum_n P_n E_n \tag{3.22}$$

$$C_v = \frac{1}{k_B T^2} \sum_n P_n (E_n - U)^2 \tag{3.23}$$

In Figure 3.2, we present a plot of excitation energies of FArO and FO for a total of 54 low-lying states. For the CASCI calculation of FO molecule, all low-lying excited states

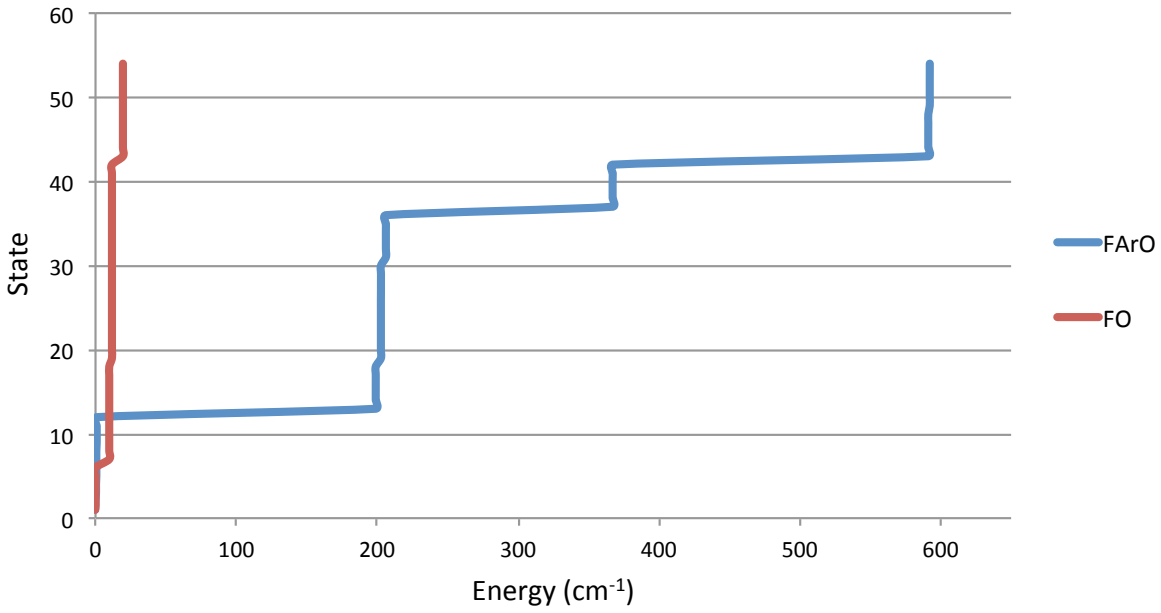

Figure 3.2: The excitation energies curve of FArO and FO molecules obtained using the CASCI.

are located within 20 cm^{-1}. However, for the CASCI calculation of FArO molecule, the excitation energies for these low-lying states range from $0 \sim 600$ cm^{-1} with four basic energy splittings, which indicates that the excitation energies are sensitive to the inclusion of the Argon atom which acts as a spacer. To test the effect of spin-orbit coupling, we also investigate the excitation energies and heat capacity plots for FArO using the CASCI and SOC_CASCI. In Figure 3.3, the excitation energies plot and heat capacity plot indicate that CASCI and SOC_CASCI calculations are quite different. In particular, the inclusion of SOC gives rise to a smearing of the energy levels. Moreover, the energy difference between the lowest and highest magnetic level increases significantly from 600 cm^{-1} to around 970 cm^{-1}. This indicates that the Argon atom and SOC are extremely important for the magnetic energy level spacing.

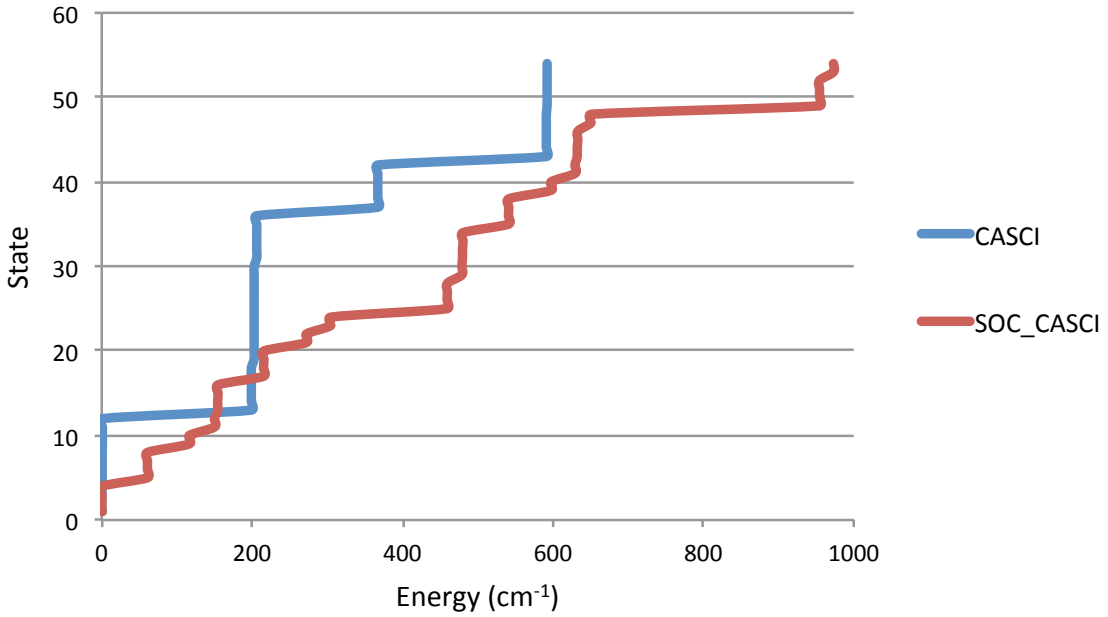

(a)

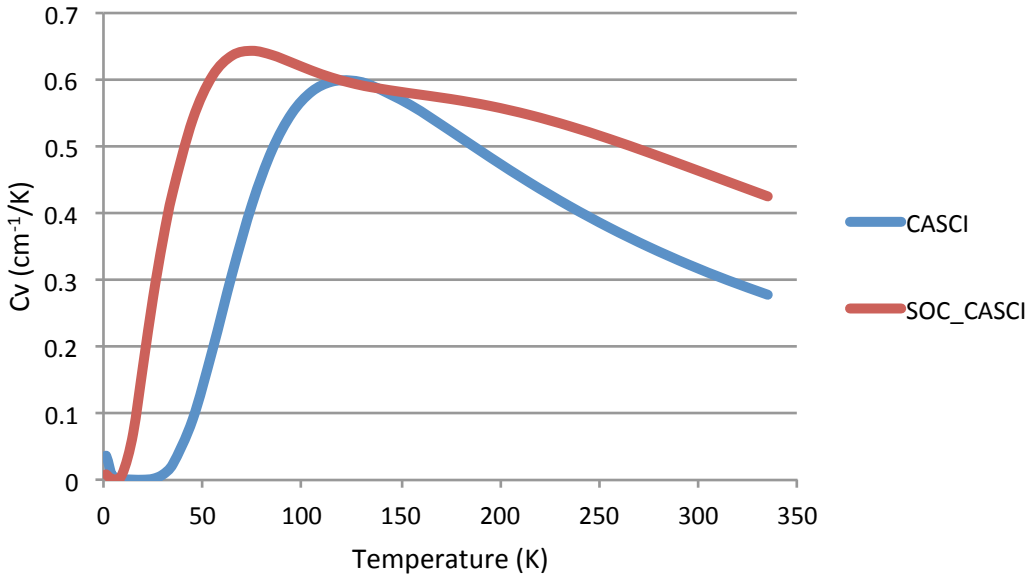

(b)

Figure 3.3: Plots of (a) excitation energies and (b) heat capacity for FArO using the CASCI and SOC_CASCI.

3.4.1.2 Determination of the Effect of Dynamical Correlation

In the previous section, the qualitative performance based on the CAS level has been discussed. Those results support our motivation to explore this further in terms of the dynamical correlation contribution on our statistical-mechanical properties of the low-lying excited states. Here, we first report the performance of the SOC_CASCI and SOC_MRCISD + Q for FArO molecule at bond length R = 2.9 Å. In Figure 3.4, it is clear that the shapes of excitation energies plot and heat capacity plot are qualitatively similar, which indicates that the contribution from dynamic correlation is not large, but it is still important for quantitative accuracy [60]. As has been discussed in refs. [3, 12, 14, 15], MRCISD+Q approach is considered to be fairly efficient but it is not rigorously size-consistent. MRCISD+Q method rapidly becomes expensive if the size of the molecule gets larger and in particular if the number of magnetic sites increase. MREOM approaches scale in a better way and are applicable to larger systems because of the reduced final diagonalization space. As a result, it is of interest to make a comparison among the SOC_MRCISD + Q, SOC_MREOM and SOC_MREOM_1p1h calculations. In Figure 3.5, the excitation energies plot and heat capacity plot for SOC_MRCISD + Q are seen to be closely comparable to those of SOC_MREOM and SOC_MREOM_1p1h for FArO molecule at R = 2.9 Å. This shows that MREOM approaches are convincingly accurate enough compared to MRCI+Q approach. Also, the slight difference between SOC_MREOM and SOC_MREOM_1p1h approaches indicates that the inclusion of the ph and 2h excitations is not significant. It is also interesting to note that in Figure 3.5, there is a small peak at $T = \sim 5K$ for SOC_MRCISD + Q approach in the heat capacity plot, which is not visible in the SOC_MREOM and SOC_MREOM_1p1h results. This peak arises because there are two

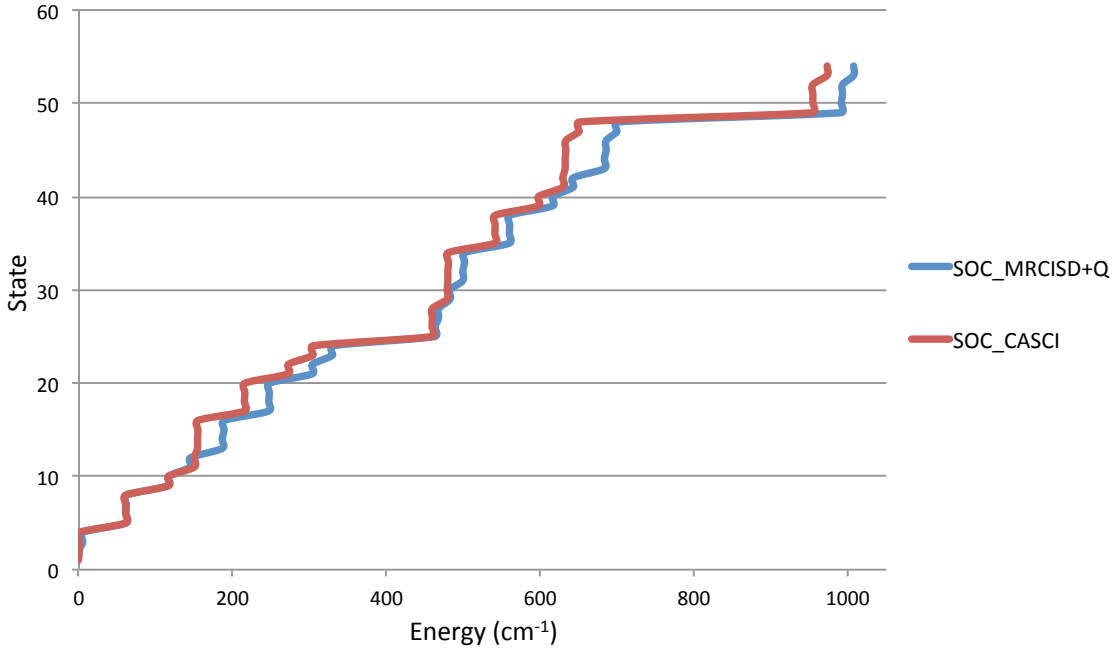

(a)

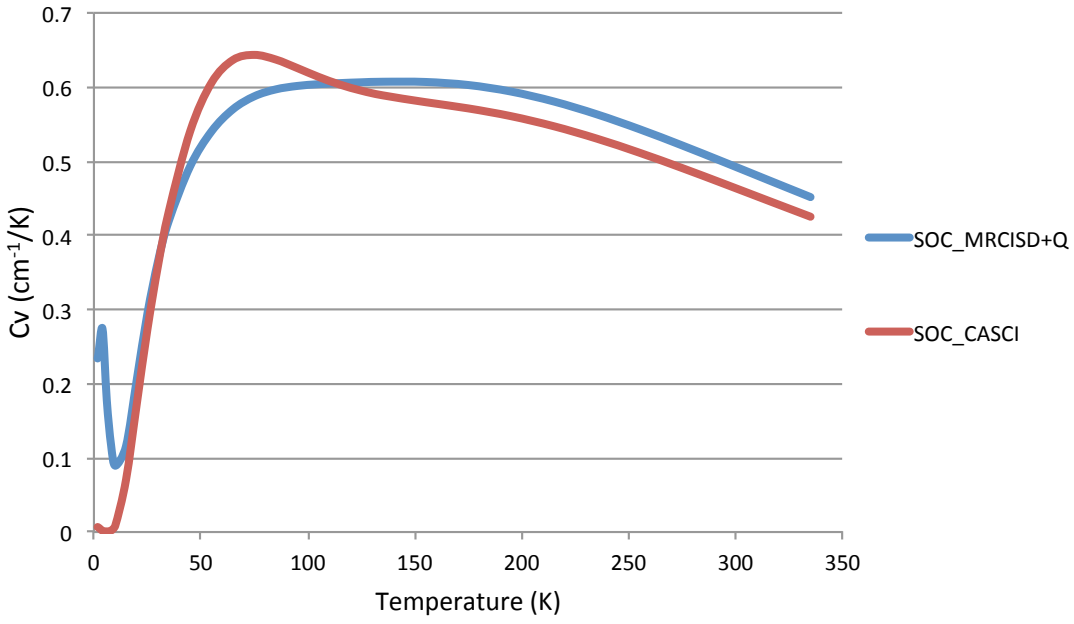

(b)

Figure 3.4: Plots of (a) excitation energies and (b) heat capacity for FArO using the SOC_CASCI and SOC_MRCISD+Q.

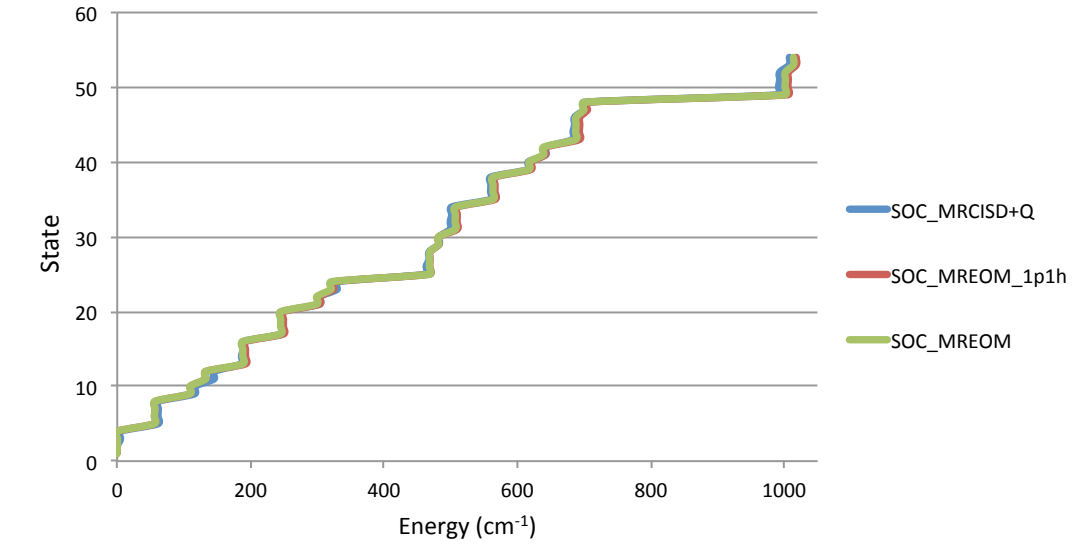

(a)

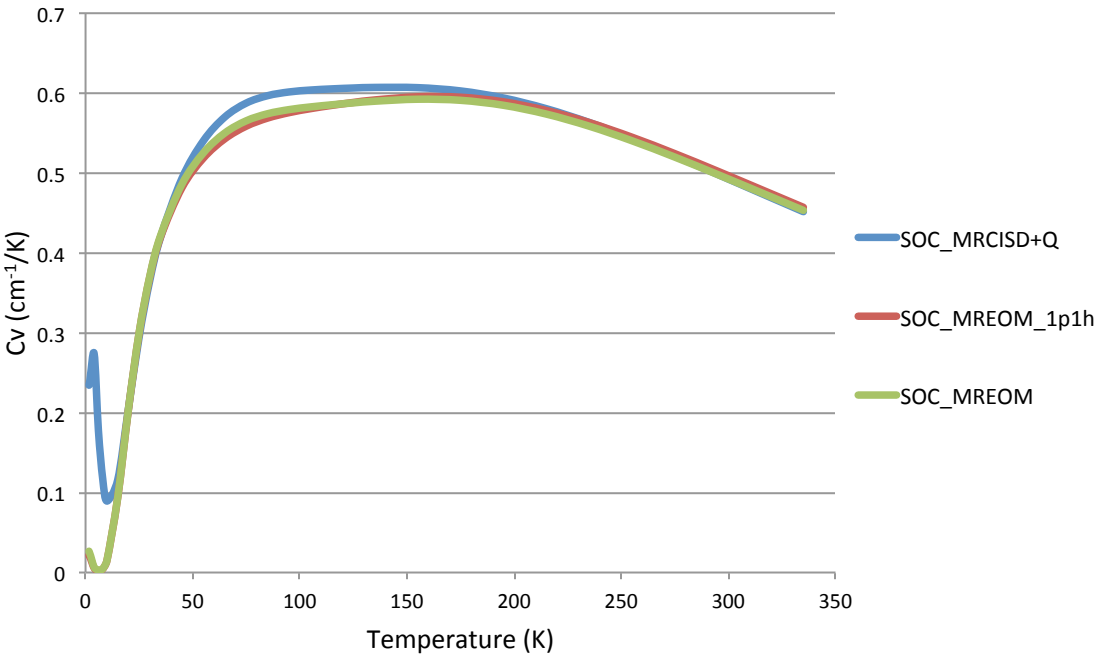

(b)

Figure 3.5: Plots of (a) excitation energies and (b) heat capacity for FArO using the SOC_MRCISD+Q, SOC_MREOM and SOC_MREOM_1p1h.

low-lying excited states sitting at 5 cm^{-1} for SOC_MRCISD + Q calculation, while the two corresponding states energies are 0.3 cm^{-1} and 0.5 cm^{-1} for SOC_MREOM and SOC_MREOM_1p1h, respectively. This illustrates that such a small difference can have significant effects at low temperatures.

3.4.1.3 Consideration of the Magnetic Coupling Effect

Our next qualitative analysis concerns the effect of magnetic coupling or the difference between interacting and non-interacting atoms. In this case, we compare the total excitation energies (in cm^{-1}) of magnetic dimer FArO molecule with the sum of excitation energies of

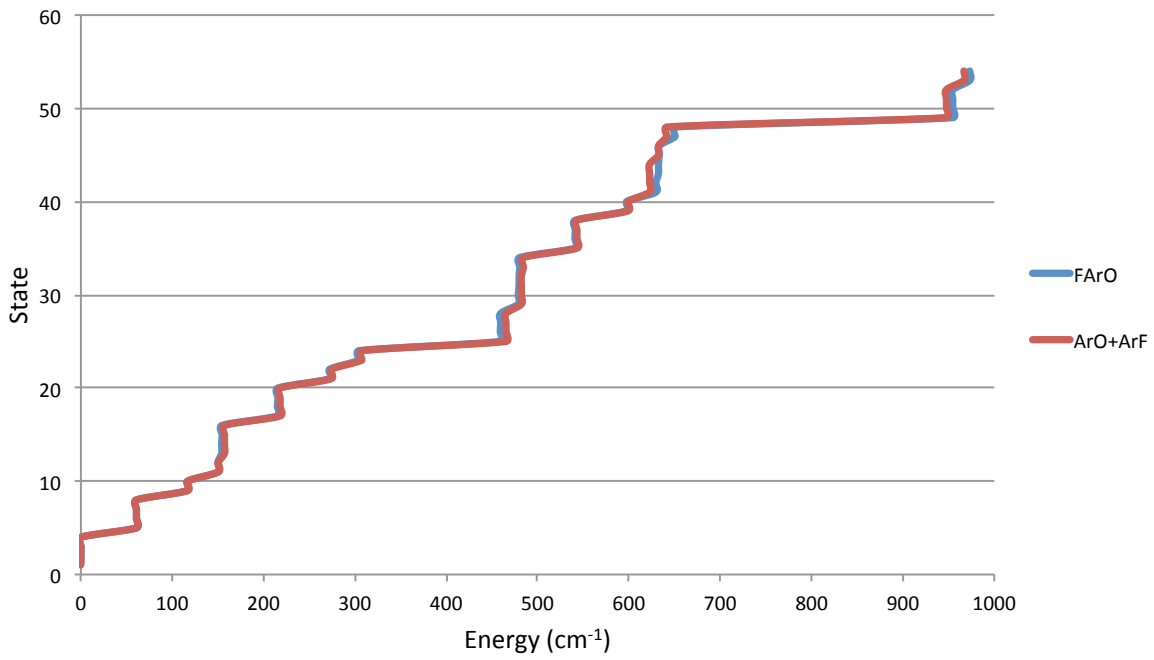

Figure 3.6: The excitation energies curve of interacting molecule (FArO) and non-interacting molecules (ArF+ArO) using the SOC_CASCI.

ArF and ArO magnetic monomer molecules for each corresponding low-lying excited state. In Figure 3.6, the excitation energies plots show that the energy levels between interacting and non-interacting systems quite nearly match each other. This indicates that the true magnetic coupling effects in the model systems are small. They strongly depend on the interatomic distance, as will be discussed later.

3.4.1.4 A Test of Accuracy: Size-consistency

As has been reported in section 3.4.1.2, there is very little difference between MRCI and MREOM approaches if one simply looks at these excitation energies and heat capacity plots. Let us take a deeper look, however, at the magnetic coupling effect in a quantitative perspective. To test the accuracy of MRCI and MREOM methods as well as to clearly see the effect of size-consistency, we look at the excitation energies difference between interacting and non-interacting moieties.

Let us here define the two-body energy, which can be used to focus on the effects of magnetic interactions. This can be expressed as

$$\Delta E_{\lambda\nu}^{two-body} = \Delta E_{\lambda\nu} - (\Delta E_{\lambda} + \Delta E_{\nu}) \tag{3.24}$$

in which $\Delta E_{\lambda\nu}$ is the excitation energy of FArO, while ΔE_{λ} and ΔE_{ν} represent the corresponding excitation energies of ArF and ArO, respectively. The sum energies $(\Delta E_{\lambda} + \Delta E_{\nu})$ are sorted such that they correspond to magnetic excitation energies of FArO, $\Delta E_{\lambda\nu}$.

We first compare the two-body energies of FArO using the SOC_CASCI in both ORCA and Molpro package. A set of calculations containing 13 bond lengths ranging from 2.5 Å

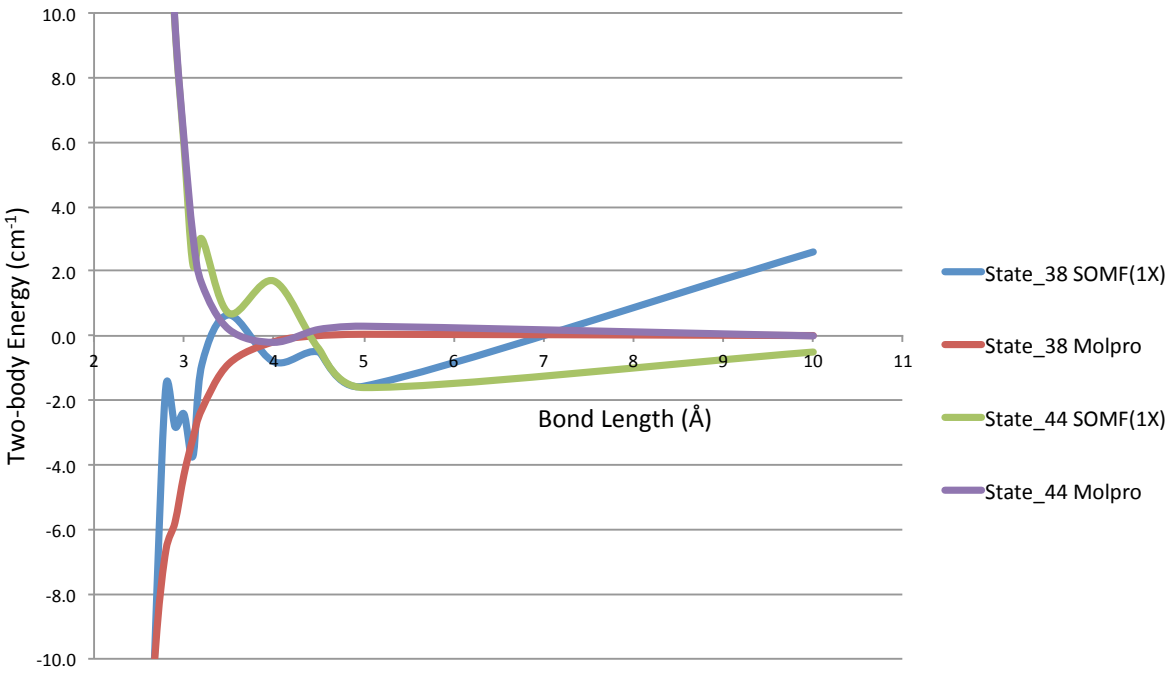

Figure 3.7: Two-body energies for FArO using default SOC_CASCI in Molpro and ORCA for states 38 and 44.

to 10 Å are performed to make a detailed comparison. Quite surprisingly, it is observed in Figure 3.7 that the default SOC approach denoted as SOMF(1X) in ORCA lacks of rigorous size-consistency as the asymptote does not go towards 0 cm^{-1}, for example for states 38 and 44. This issue with size-consistency in default ORCA SOC calculations using SOMF(1X) is due to the definition of the state-averaging. By default only states are included that are almost exactly degenerate. For FArO only one state is included, unless the distance is very large. However, for the linear molecules ArF and ArO, two states are included since the π states are doubly degenerate. This significantly affects SOC in the mean field approximation, and this causes the unexpected behavior. The solution to the

problem for these particular systems is fairly straightforward: we include all 54 magnetic states in the definition of the average density that enters the SOMF(1X) procedure. An alternative procedure would be to use the states that are used in the high-spin CASSCF. This could be a most satisfactory general solution, but this requires a more substantial change to the ORCA code, and this is not pursued here. ORCA calculation will be performed under m_SOMF(1X) again to test the size-consistency issue. In Figure 3.8, it can be seen that the size-consistency error in SOC_CASCI is fixed using the m_SOMF (1X) approach. In a further step, to test the size-consistency issue with inclusion of correlation energies,

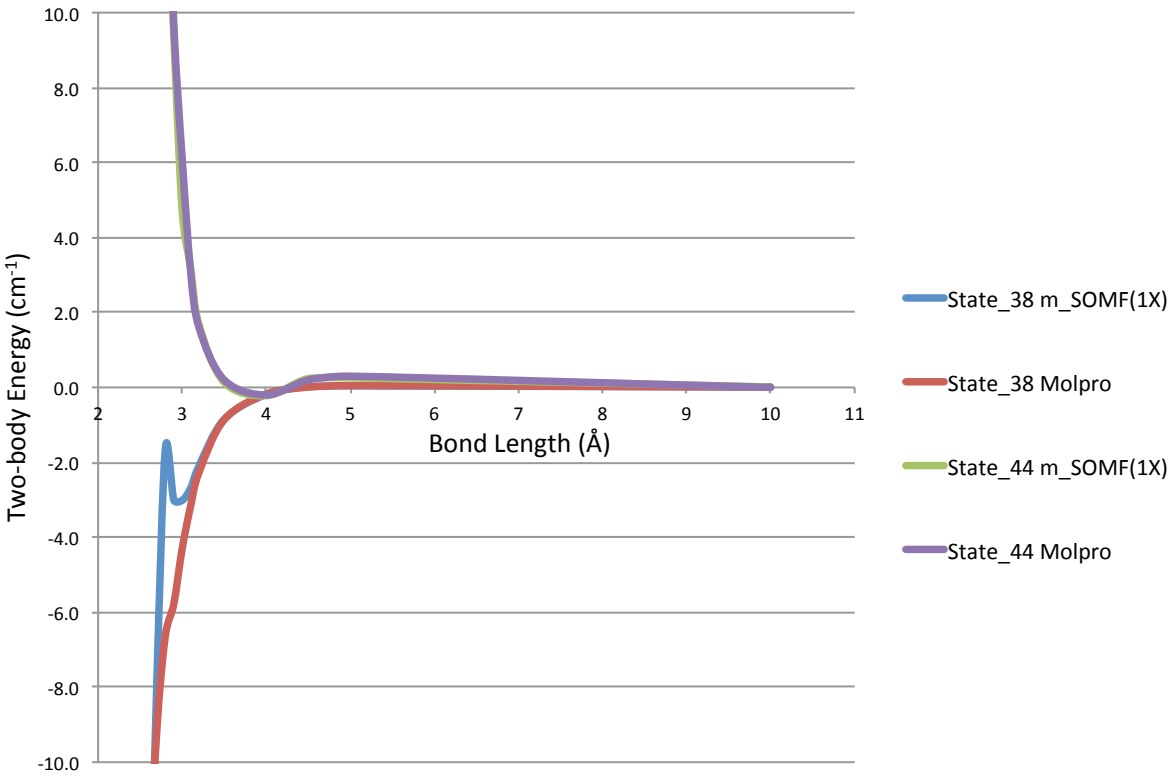

Figure 3.8: Two-body energies for FArO using default SOC_CASCI in Molpro and m_SOMF(1X) in ORCA for states 38 and 44.

we perform SOC_MRCISD + Q and SOC_MREOM calculations on FArO molecule at the same 13 bond lengths. In all SOC_MREOM calculations reported in this paper (including previous section 3.4.1.2), we used the modified SOMF(1X) to include SOC. Figure 3.9 shows the behavior of two-body energies for states 40 and 47. As anticipated, the asymptote of MREOM approach is perfect at 0 cm^{-1}, as it is a nearly size-consistent method. One also observes that SOC_MRCISD + Q approach does not yield reasonable results, as the asymptote is not flat at 0 cm^{-1} at larger bond distances. This clearly illustrates the violation of size-consistency.

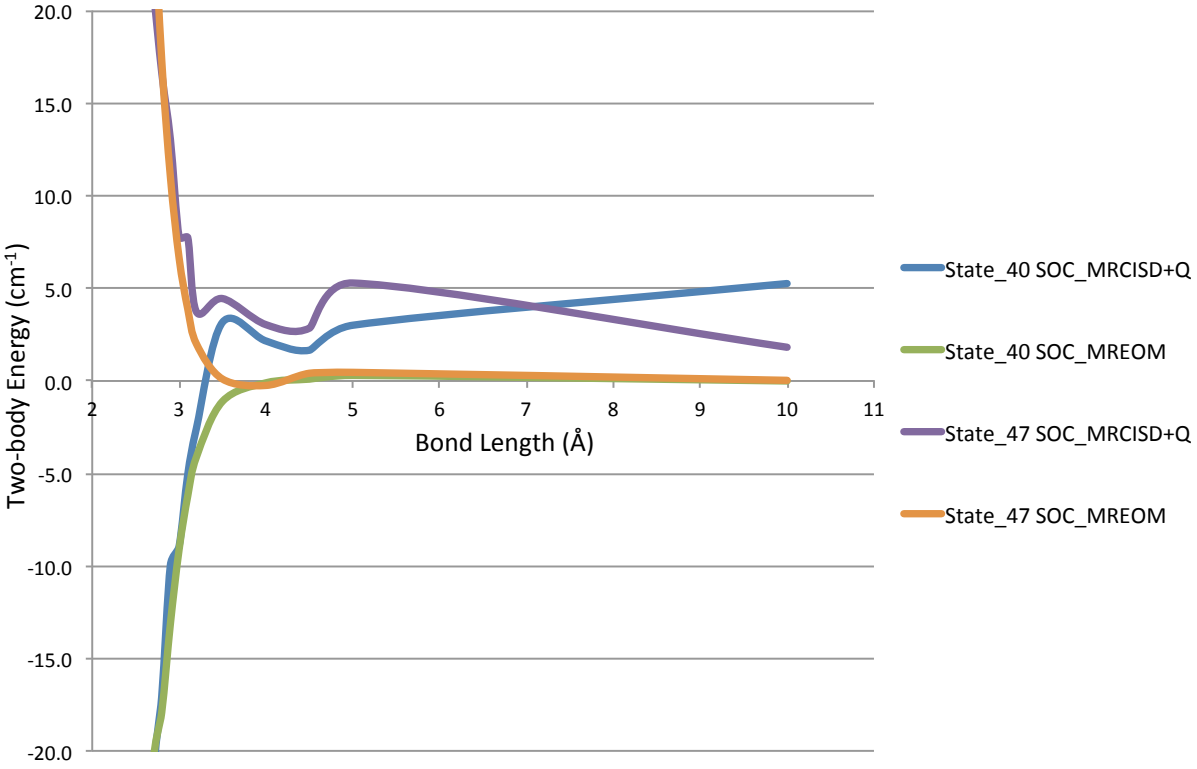

Figure 3.9: Two-body energies for FArO using the SOC_MRCISD+Q and SOC_MREOM for states 40 and 47.

3.4.1.5 Determination of the Behavior of Excitation Energies for FArO at Smaller Bond Distances

Let us again look at the analysis of excitation energies for FArO. In Figure 3.10, we report the excitation energies plot for excited state 28 with respect to the increase of bond length using the SOC_MREOM. The plot indicates that the excitation energy is nearly converged

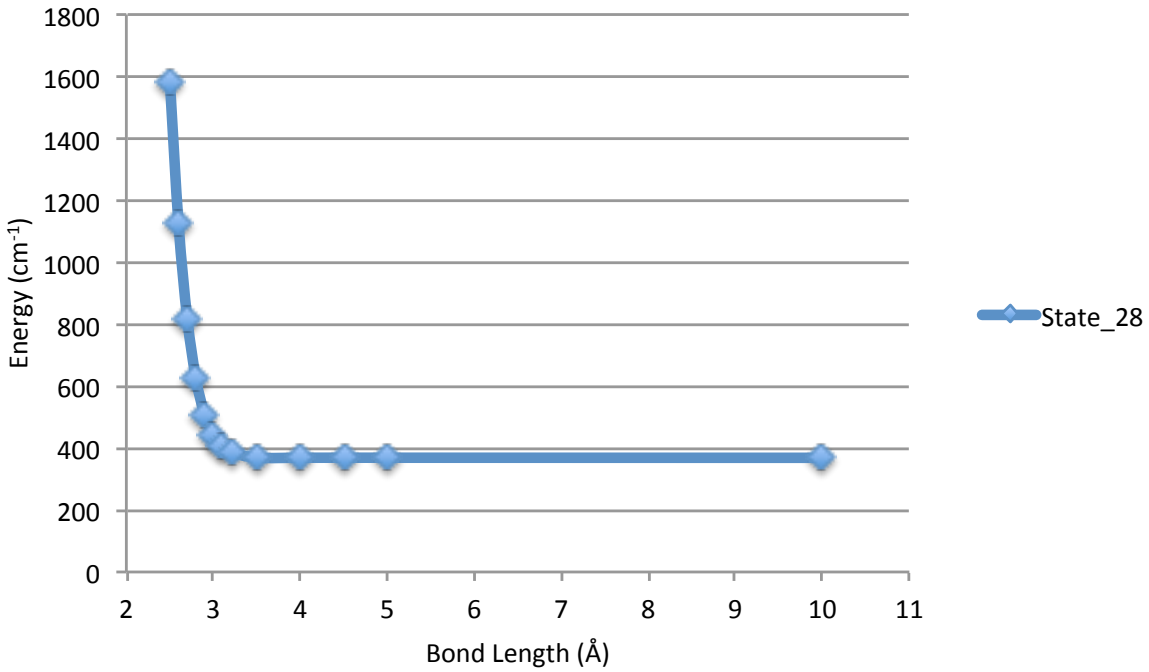

Figure 3.10: Excitation energies for state 28 of FArO molecule obtained using the SOC_MREOM.

at bond length R = 3.1 Å, and definitely converges at R = 10.0 Å. This result supports our motivation for performing a more detailed analysis on the behavior of excitation energies for FArO at smaller bond lengths. Table 3.2 shows the molecular excitation energies of 9 low-lying excited states using the SOC_MREOM. In Figure 3.11, we explore the quadratic and

State	R=2.5Å	R=2.6Å	R=2.7Å	R=2.8Å	R=2.9Å	R=3.0Å	R= 3.1Å	R=10.0 Å
17	1315.9	849.7	534.5	326.3	193.0	110.4	60.7	0.0
21	1379.1	912.7	596.2	385.8	249.1	161.5	104.4	0.0
25	1446.3	980.3	665.2	457.0	323.7	241.1	191.4	130.7
29	1581.2	1122.9	818.7	624.2	507.6	440.4	404.8	368.6
33	1644.3	1185.8	880.2	683.6	562.5	491.1	447.6	368.6
37	1711.4	1253.3	946.2	755.3	638.0	571.4	535.5	499.4
43	1906.7	1351.4	954.9	685.0	481.1	354.3	277.6	196.1
49	3337.7	2285.2	1549.5	1043.5	703.8	483.5	350.1	196.1
54	3601.1	2556.1	1830.7	1337.9	1013.5	809.8	690.4	564.7

Table 3.2: Molecular excitation energies for a number of excited states of FArO molecule using the SOC_MREOM. All results are in cm^{-1}.

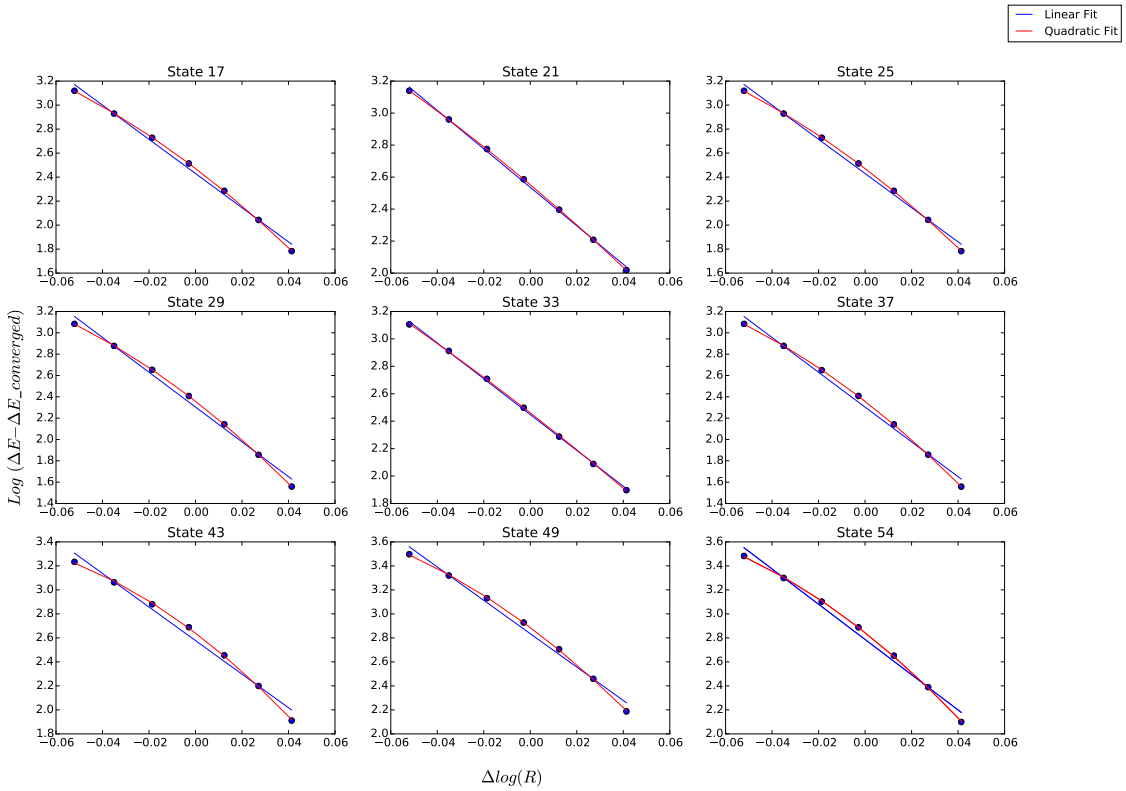

Figure 3.11: Quadratic fit and linear fit plots of log (ΔE − ΔE_converged) versus Δlog (R) for a number of excited states of FArO molecule obtained using the SOC_MREOM.

linear relationship between log (ΔE − ΔE_converged) and Δlog (R), where ΔE_converged is the converged excitation energy at R=10 Å, and Δlog (R) is given by log (R) - 0.45. It is seen that the quadratic curve provides an excellent fit to the data. The stability of the fit indicates the robustness of MREOM results with regard to a change in bond length, and size-consistency is mandatory to achieve such a result. In Table 3.3, the linear expansion coefficients of the two fits for these 9 excited states are reported. It is clear that the linear coefficient for these two fits are quite comparable. From the linear fit, we can extract a scaling law $\Delta E \sim R^{-X}$, where X ranges from 12 to 16, depending on the state. Let us emphasize that it is hard to get some theoretical estimate of the R-dependence of ΔE, as ΔE is the two-body effect in the excitation energy. The prime purpose of this section is to illustrate the robustness of MREOM, indicating that MREOM is suitable to explore the strength of magnetic coupling for different scenarios.

States	Quadratic Fit	Linear Fit
17	-14.71	-14.25
21	-12.21	-12.03
25	-14.71	-14.25
29	-16.93	-16.32
33	-13.20	-13.06
37	-16.91	-16.31
43	-14.69	-13.99
49	-14.68	-13.91
54	-15.32	-14.68

Table 3.3: Comparison of the linear expansion coefficients for quadratic fit and linear fit.

3.4.2 Results for Larger Systems

Here we will explore further to two larger artificial systems: FArOF and FArOFH. The geometric structures of these two molecules are presented in Figure 3.12. The total number of low-lying excited states for FArOF and FArOFH is 324 and 648, respectively. Therefore, the SOC_MRCISD+Q calculation is quite expensive and is not available in this work. Instead, we perform the SOC_MREOM calculation for these magnetic molecules. The full SOC_MREOM calculation for FArOF and FArOFH takes about 2 CPU hours and 2 CPU days, respectively, on a single processor of a 12-core node, consisting of Intel XEON 2.93 GHz CPUs with 12.3 MB of shared cache memory. The excitation energies plot and heat capacity plot for FArOF and FArOFH are illustrated in Figure 3.13 and Figure 3.14, respectively. This indicates the applicability of MREOM approaches for large magnetic systems.

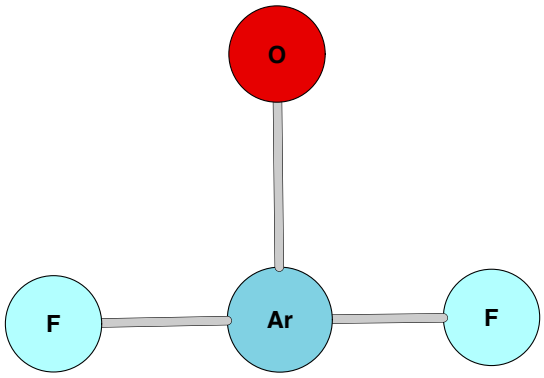

(a)

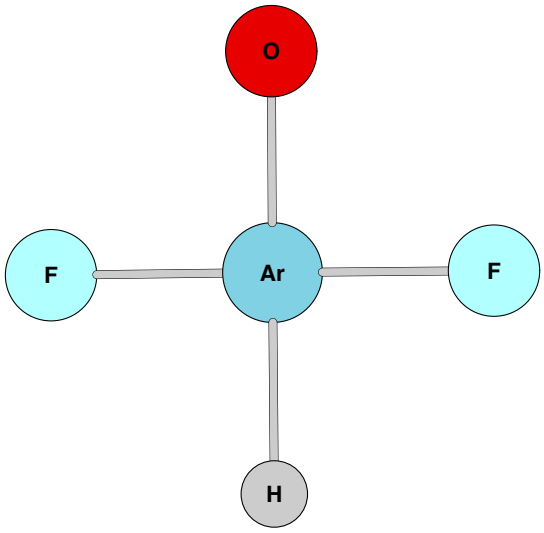

(b)

Figure 3.12: The geometric structure of (a) FArOF and (b) FArOFH molecules. All bond lengths are identical. All bond angles are 90°.

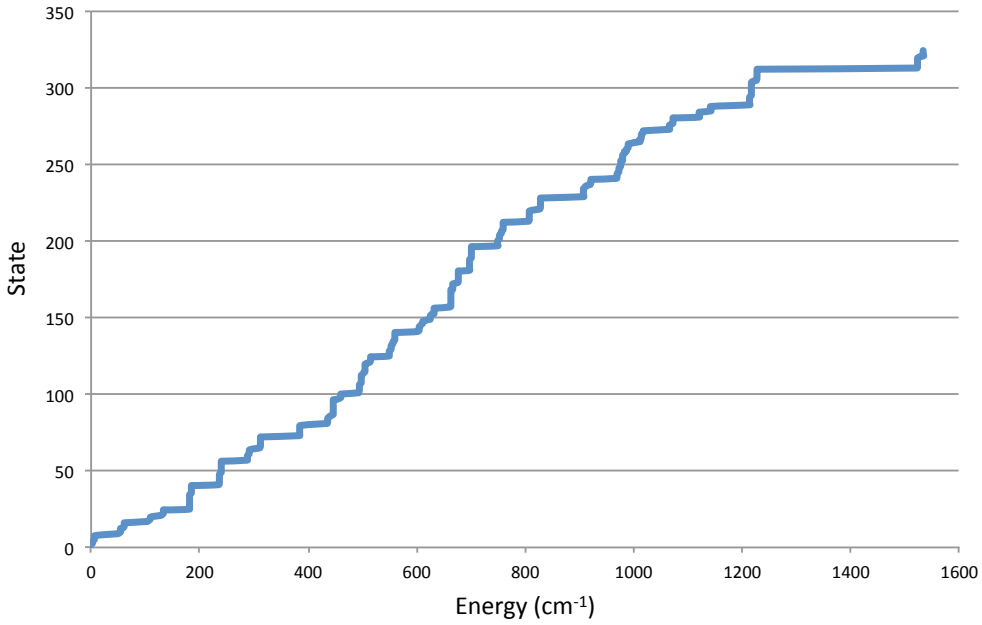

(a)

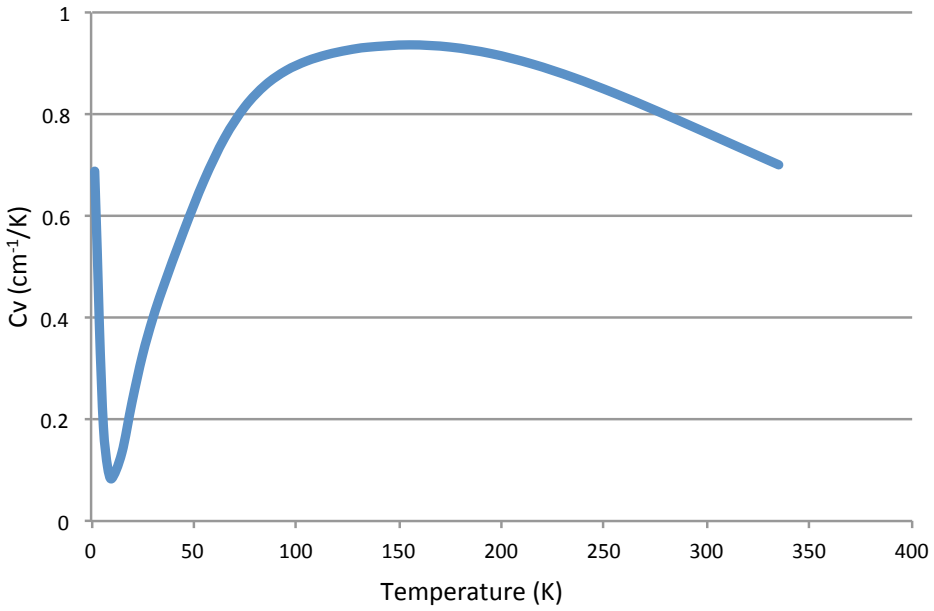

(b)

Figure 3.13: Plots of (a) excitation energies and (b) heat capacity for FArOF using the SOC_MREOM. R = 2.9 Å.

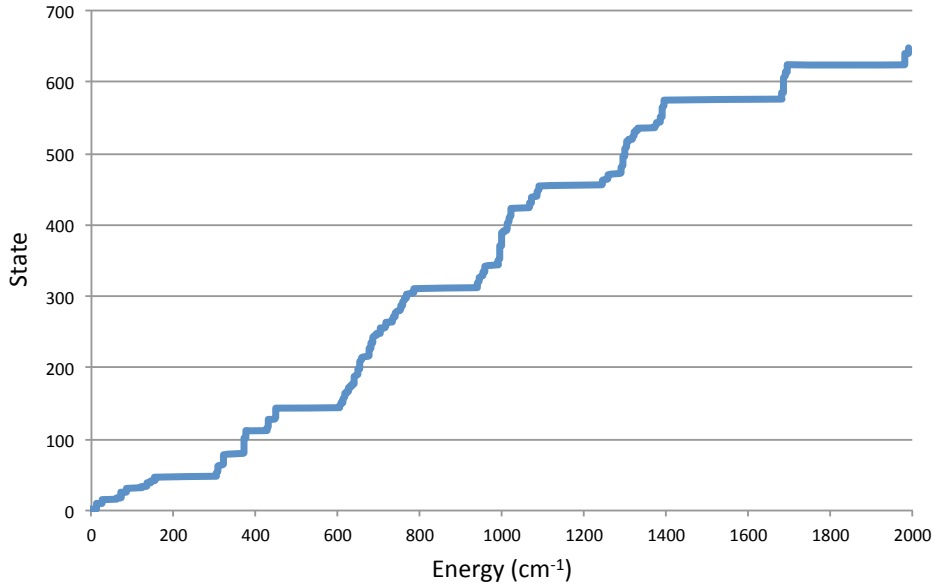

(a)

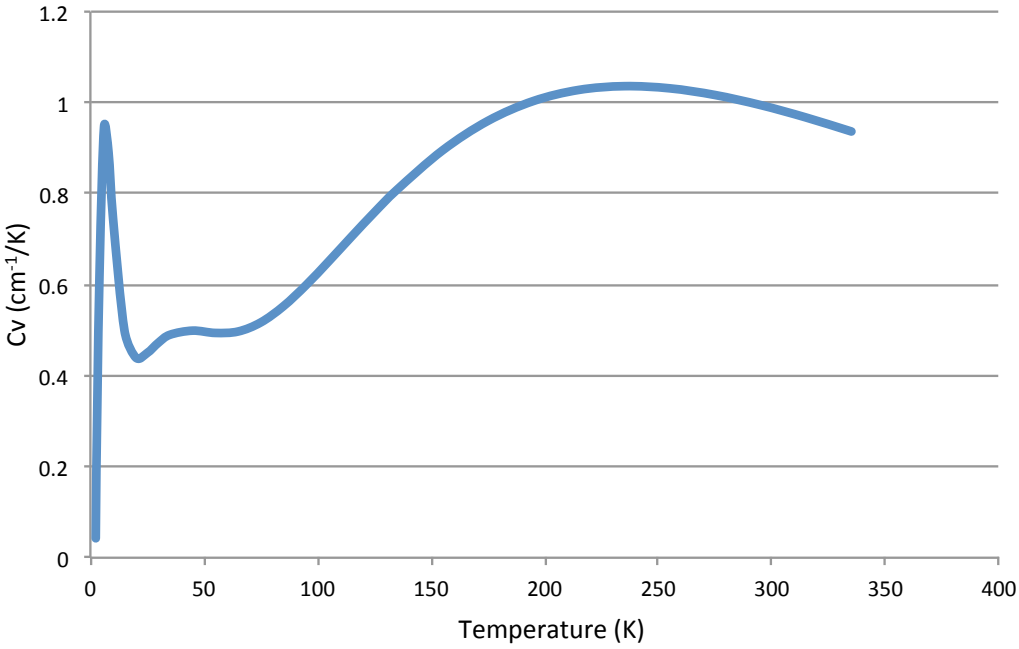

(b)

Figure 3.14: Plots of (a) excitation energies and (b) heat capacity for FArOFH using the SOC_MREOM. R = 2.8 Å.

3.5 Conclusion

In this work, we established the accuracy of the MR-EOM-T|T†|SXD|U approach implemented in the ORCA program, in conjunction with a modified SOMF(1X) inclusion of spin-orbit coupling. The primary advantage of MREOM is the computational efficiency for systems that have many (hundreds) of electronic states, but which share the same active space. Magnetic systems can be considered as prototype examples to illustrate the merits of MREOM. Even though MREOM is not strictly size-consistent, in practice this is of no concern for systems of this type. The computational scaling of MREOM is not fundamentally different from MRCI, and one cannot push the methodology to a very large number of magnetic atoms. However, the method is sufficiently effective such that one can treat system with up to about four magnetic sites of arbitrary spin S. Therefore, one can treat magnetic coupling beyond two-body effects. In this paper, we have only tested the applicability of the approach for artificial model systems. A next step would be the application to move realistic models of magnetic materials, and the extraction of magnetic model parameters along the lines discussed in refs. [3, 28].

Chapter 4

Effective Hamiltonian Approach to Magnetic Model Systems

As reported in the previous chapter, the computational cost using a strongly correlated method, for example, SOC_MREOM, for magnetic model system FArOFH is around 2 CPU days. The most time-consuming step in MREOM for such magnetic systems with very many low-lying states in the diagonalization of the transformed Hamiltonian over the CAS, 1p and 1h space. This will limit the applicability of the methodology. For this reason, it is of interest to design more efficient methods to treat this final diagonalization step that capitalize on the fact that much is known about the structure of the problem. In this chapter, we assume we can extract a model Hamiltonian that describes interaction between pairs of magnetic units, using a suitable basis of slater determinants. For small systems, this model Hamiltonian can be diagonalized exactly. Our interest is to construct an effective Hamiltonian method that upon diagonalization yields good approximation

to the low-lying states energies of interest, which is significantly more efficient than the diagonalization of the full magnetic Hamiltonian.

The effective Hamiltonian theory was initially formalized by Bloch and des Cloizeaux [24, 25], and has been explained in many works [61, 62, 63, 64, 65]. In general, most model Hamiltonians are constructed based on the large energy gap between the localized ground states and excited states of a magnetic system such that one can restrict the model Hamiltonian to a compact space of low-lying configurations. The studies discussed hereafter present a so-called *effective Hamiltonian approach* to obtain low-lying states for a Hamiltonian including pair interaction only. This chapter is exploratory in nature, and at this stage, we neglect the inclusion of spin-orbit coupling and dynamical correlation. The starting point would be a CASSCF calculation [40]. We first give a brief introduction to the features of magnetic model systems in this work, and then describe the details of effective Hamiltonian approach with its variants. Finally, the approach with its variants are performed to some suitable magnetic systems to test the accuracy.

4.1 Introduction to Magnetic Model Systems

To illustrate the goal of the approach discussed in this chapter, let us first introduce some artificial magnetic systems that cannot be made experimentally, such as Ar_2N_3, Ar_2O_3, Ar_2Cr_3. They serve as illustrations and useful model systems. These systems are described as open-shell systems, as nitrogen, oxygen and chromium atoms all have unpaired electrons. In addition, the spin of unpaired electrons can create a magnetic field; as a result, each N, O, Cr, atom is considered as a magnetic site. Meanwhile, Ar atom acts as a spacer. The

geometry of the system is designed such that the magnetic atoms are well separated.

For each magnetic system, we would like to preserve a fixed number of particles on each magnetic site, or equivalently we will neglect ionic configurations. At the level of the second-quantized Hamiltonian, that is, the number of creation and annihilation operators for each site should be equal. We assume in this proposal that

$$h_p^r = 0, \quad \text{unless}\,(p,r) \in (i) \tag{4.1}$$

$$h_{pq}^{rs} = 0, \quad \text{unless}\,(p,q,r,s) \in (i)\,\text{or}\begin{cases} (p,r) \in (i),\ (q,s) \in (j) \\ (p,s) \in (i),\ (q,r) \in (j) \end{cases} \tag{4.2}$$

Here we use indices i, j to label two different magnetic sites. Localized orbitals centered on magnetic sites are labelled as p, q, r, s. As a result, neutral configurations cannot couple to ionic configurations. This setting to zero of matrix elements is to be accomplished by a similarity transformation. We will here assume it to be accomplished and will not discuss it further. Then, the ionic terms can all be excluded, after the transformation.

The new neutral Hamiltonian in a complete active space (CAS) is given by

$$\begin{aligned}\hat{H} = &\sum_i \sum_{p,p'} h_{p'}^{p} \hat{p}^\dagger p' + \frac{1}{2}\sum_i \sum_{p_1,p_2,p_3,p_4} h_{p_1p_2}^{p_3p_4} \hat{p}_3^\dagger \hat{p}_4^\dagger \hat{p}_2 \hat{p}_1 \\ &+ \frac{1}{2}\sum_{i,j} \sum_{p,q,p',q'} h_{p'q'}^{pq} \hat{p}^\dagger \hat{q}^\dagger q' p' + \frac{1}{2}\sum_{i,j} \sum_{p,q,p',q'} h_{p'q'}^{qp} \hat{q}^\dagger \hat{p}^\dagger q' p'\end{aligned} \tag{4.3}$$

The notations $p, p', p_1, p_2, p_3, p_4$ denote localized orbitals on site i, while q, q' indicate localized orbitals on site j.

The fourth term in Eq. (4.3) is the exchange term arising from the two-body integral. The

spin can be exchanged between two sites during the operation.

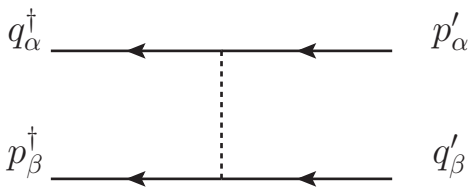

Figure 4.1: Diagram representing the exchange interaction.

In order to investigate the magnetism of these model systems, the properties with regard to the electronic configuration of each atom should be described first. We define low-lying states corresponding to different atoms (or sites) $i, j, k, l, \cdots$ as $|I\rangle, |J\rangle, |K\rangle, |L\rangle, \cdots$, and high-lying states are denoted as $|A\rangle, |B\rangle, |C\rangle, |D\rangle, \cdots$ while the general states are labelled as $|P\rangle, |Q\rangle, |R\rangle, |S\rangle, \cdots$, respectively. Likewise, if there is more than one state, we can use the general labels $|I'\rangle, |J'\rangle, |K'\rangle, |L'\rangle, \cdots$, for the low-lying states, $|A'\rangle, |B'\rangle, |C'\rangle, |D'\rangle, \cdots$, standing for high-lying states, and $|P'\rangle, |Q'\rangle, |R'\rangle, |S'\rangle, \cdots$, describing general states for each different site. For example, if we take one single nitrogen atom into consideration, there are 20 microstates, which can be labelled as $|P\rangle$. The atomic term symbol for the low-lying level (4 states) is ^4S, and can be denoted as $|I\rangle$. We have 4 out of 20 states accounted for. The remaining multiplets are ^2D, ^2P with 16 states, which are represented by $|A\rangle$.

In a further step we define the neutral Hamiltonian in configuration space (as will be discussed in section 4.2), which is written as

$$\hat{H} = \sum_i \sum_{P,P' \in i} H_P^{P'} |P'\rangle\langle P| + \sum_{i<j} \sum_{P,P' \in i} \sum_{Q,Q' \in j} H_{PQ}^{P'Q'} |P'Q'\rangle\langle PQ| \tag{4.4}$$

In general, the molecular states in the basis of configurations are defined as

$$|\Psi\rangle = \sum_{P\in i}\sum_{Q\in j}\sum_{R\in k}\sum_{S\in l}\sum_{\ldots}|PQRS\cdots\rangle C_{PQRS\ldots} \tag{4.5}$$

To continue our discussion on our magnetic systems, we first give the electronic configuration for some representative atoms in Table 4.1.

Atom-Type	Ground States Symbol	Degeneracy	Number of Neutral States Per Atom
N	^4S	4	$\binom{6}{3} = 20$
O	^3P	9	$\binom{6}{4} = 15$
Cr	^7S	7	$\binom{12}{6} = 924$

Table 4.1: Electronic configuration for three different atoms.

Then, we can quantitively explore the microstates of the magnetic model systems Ar_2X_3, X=N, O, Cr in Table 4.2.

Molecule	Total Valence States	Total Neutral States	Total Low-lying States
Ar_2N_3	$\binom{18}{9} = 48620$	$20^3 = 8000$	4^3=64
Ar_2O_3	$\binom{18}{12} = 18564$	$15^3 = 3375$	9^3=729
Ar_2Cr_3	$\binom{36}{18}$=9.07E+09	924^3=7.89E+08	7^3=343

Table 4.2: Microstates for Ar_2X_3 X=N, O, Cr.

Our aim is to reduce the size of the full space of complete active space self-consistent field (CASSCF) [40] dimension, to that of the the low-lying states. For example, the number of valence states is 48620 for Ar_2N_3, which results in a total number of 48620^2=2.36E+09 matrix elements in the calculation, while the number of matrix elements is 64^2=4096 con-

sidering only the low-lying states calculation. As a result, we need to find an appropriate approximation to investigate these magnetic systems.

4.2 Construction of Configurational Magnetic Hamiltonian

To calculate the matrix element of the magnetic Hamiltonian over neutral configurations, special procedures have been incorporated in the ACES II program [66]. In the first stage of the calculations, a state-averaged CASSCF/CASCI calculation is done such that all relevant configurations of the atom are included. Upon convergence of the CASSCF calculations, the active space orbitals are localized on the magnetic atoms. This is accomplished quite readily and the resulting orbitals are localized and orthonormal. In a subsequent calculation, the configurational matrix-elements are obtained. To obtain the one-body matrix element $H_P^{P'}$ as shown in Eq. (4.4), one simply constructs all neutral configurations $|P\rangle$, and evaluates matrix-elements of the Hamiltonian. By construction only the first two terms in Eq. (4.3) can contribute. We also evaluate the full two-body Hamiltonian matrix $H_{PQ}^{P'Q'}$ over all neutral configurations $|PQ\rangle$. These matrix elements would involve contributions from all elements in Eq. (4.3) localized on sites i and j. To get the one- and two-body parts of the magnetic Hamiltonian matrix, one obtain

$$H_{PQ}^{P'Q'} = M_{PQ}^{P'Q'} - \delta_P^{P'} H_Q^{Q'} - H_P^{P'} \delta_Q^{Q'} \tag{4.6}$$

This procedure is repeated for all pairs of magnetic sites $i < j$ and the matrix elements are then written to a file. This file is read by the program that performs the effective Hamiltonian calculations.

4.3 Brief Outline of the Effective Hamiltonian Approach

We assume that the molecular magnetic Hamiltonian is expressed as

$$\hat{H} = \sum_i \sum_{P,P' \in i} H_P^{P'} |P'\rangle\langle P| + \sum_{i<j} \sum_{P,P' \in i} \sum_{Q,Q' \in j} H_{PQ}^{P'Q'} |P'Q'\rangle\langle PQ| \tag{4.7}$$

The zero order wavefunction for low-lying states is written as

$$|\Psi_{IJKL\cdots}\rangle = \sum_{I \in i} \sum_{J \in j} \sum_{K \in k} \sum_{L \in l} \sum_{\ldots} |IJKL\cdots\rangle C_{IJKL\cdots} \tag{4.8}$$

where $C_{IJKL\cdots}$ is the CI coefficient in space of low-lying states.

To describe the full wavefunction including the (small) contribution from high-lying configurations, we use the ansatz:

$$|\Psi\rangle = \sum_{I \in i} \sum_{J \in j} \sum_{K \in k} \sum_{L \in l} \sum_{\ldots} \left\{ e^{\hat{T}} \right\} |IJKL\cdots\rangle C_{IJKL\cdots} \tag{4.9}$$

Here, the normal-ordered exponential $\left\{ e^{\hat{T}} \right\}$ is employed such that we do not consider terms in with T-operators acting on one atomic site more than once. Hence, for example,

$\hat{T}_{IJ}^{AJ'}\hat{T}_{J'K}^{BC}$ is excluded, because the excitation operates on site j twice. The cluster operator in configuration space is defined as

$$\begin{aligned}\hat{T} &= \hat{T}_1 + \hat{T}_2 + \hat{T}_s \\ &= \sum_i \sum_{I,A\in i} t_I^A |A\rangle\langle I| + \sum_{i<j} \sum_{I,A\in i} \sum_{J,B\in j} t_{IJ}^{AB} |AB\rangle\langle IJ| \\ &+ (\sum_{i,j} \sum_{I,A\in i} \sum_{J,J'\in j} t_{IJ}^{AJ'} |IJ\rangle\langle AJ'| + \sum_{i,j} \sum_{I,I'\in i} \sum_{J,B\in j} t_{IJ}^{I'B} |IJ\rangle\langle I'B|)\end{aligned} \tag{4.10}$$

It is of importance to note here that $\hat{T}_s$ is denoted as two-body semi-internal operator, and is the combination of last two terms in Eq. (4.10).

Let us assume for now that all T-coefficients are known, the equations will be discussed later. The Schrödinger equation with respect to low-lying states in Eq. (4.9) can be expressed as

$$\sum_{I\in i}\sum_{J\in j}\sum_{K\in k}\sum_{L\in l}\sum_{...} \hat{H}\left\{e^{\hat{T}}\right\}|IJKL\cdots\rangle C_{IJKL\cdots} = E\sum_{I\in i}\sum_{J\in j}\sum_{K\in k}\sum_{L\in l}\sum_{...}\left\{e^{\hat{T}}\right\}|IJKL\cdots\rangle C_{IJKL\cdots} \tag{4.11}$$

and projection of this equation onto the possible low-lying configurations $\langle I'J'K'L'\cdots|$ produces a set of equations

$$\sum_{I\in i}\sum_{J\in j}\sum_{K\in k}\sum_{L\in l}\sum_{...}\langle I'J'K'L'\cdots|\hat{H}\left\{e^{\hat{T}}\right\}|IJKL\cdots\rangle C_{IJKL\cdots} = EC_{I'J'K'L'\cdots} \tag{4.12}$$

Then, we can define the *effective Hamiltonian* $\hat{G}$ over the low-lying states by

$$\hat{G} = \hat{H}\left\{e^{\hat{T}}\right\}_{low-lying} \tag{4.13}$$

$$= \left[\hat{H} + \hat{H}\left\{\hat{T}\right\} + \frac{1}{2}(\hat{H}\left\{\hat{T}^2\right\}) + \cdots\right]_{low-lying} \tag{4.14}$$

The energies of all low-lying states can be obtained through the diagonalization of the effective Hamiltonian $\hat{G}$. This yields both the energies of the low-lying states and coefficients $C_{IJKL\cdots}$ that in general will be different from the zeroth-order coefficients.

The coefficients of operator $\hat{G}$ can easily be evaluated: there can be no external virtual labels (A, B, C, D) in $\hat{G}$, which means that all virtual labels from the excitation operator $\hat{T}$ have to be summed against virtual labels from $\hat{H}$. Since virtual labels from $\hat{T}$ operators are associated with *kets*, for example, $|A\rangle$, they will be summed with the corresponding virtual labels in $\hat{H}$ represented by *bras*, for example, $\langle A|$. Since two-body matrix elements $H_{PQ}^{P'Q'}$ contain only one pair of *bra* labels, the expansion in Eq. (4.14) terminates exactly with quadratic terms, irrespective of the rank of the $\hat{T}$ operator. In addition, the only components of $\hat{T}$ operator that contribute to the quadratic terms of $\frac{1}{2}(\hat{H}\left\{e^{\hat{T}}\right\})_{low-lying}$ are $\hat{T}_1$ and $\hat{T}_s$ operators, and all elements in $\hat{G}$ are explicitly connected.

Let us now provide a brief scheme of the proposed effective Hamiltonian approach.

1. *Determine the partition into low-lying and high-lying states.*
2. *Determine the amplitudes of* $\hat{T}$.
3. *Calculate the matrix elements of* $\hat{G}$.
4. *Diagonalize* $\hat{G}$ *over low-lying configurations.*

A succinct summary to discuss each point mentioned above is given below. We will expand on each step in subsequent sections.

Step 1. To determine the low-lying and high-lying states, we will perform a mean-field calculation, which introduces a single-site density operator $\hat{D}$.

Step 2. To determine the T-amplitudes, we will consider an independent pair approximation and obtain t-amplitudes using the low-lying eigenstates of pair Hamiltonian.

Step 3. In the calculation of matrix elements of $\hat{G}$, we will introduce some renormalization ideas that essentially allow us to redefine one-, two-, three- and four-site contributions. This will use the single-site $\hat{D}$ operators.

Step 4. In the diagonalization of $\hat{G}$ we will use a direct diagonalization of the effective Hamiltonian matrix. This limits the number of sites that can be used in calculations.

4.4 Further Details of the Effective Hamiltonian Approach

4.4.1 Step 1: Mean-Field Calculation

Assume that the Hamiltonian with respect to configuration space is written as

$$\begin{aligned}\hat{H} &= \hat{H}_1 + \hat{H}_2 \\ &= \sum_i \sum_{P,P' \in i} H_P^{P'} |P'\rangle\langle P| + \sum_{i<j} \sum_{P,P' \in i} \sum_{Q,Q' \in j} H_{PQ}^{P'Q'} |P'Q'\rangle\langle PQ| \end{aligned} \tag{4.15}$$

We will try to find low-lying single-site states that are linear combinations of basis states

$$|I\rangle = \sum_P |P\rangle C_{PI} \tag{4.16}$$

This allows us to define a normalized density matrix

$$\hat{D}_P^{P'} = \frac{1}{N_I} \sum_{I=1}^{N_I} C_{PI} C_{P'I} \tag{4.17}$$

in terms of orthonormal states

$$\sum_P C_{PI} C_{PI'} = \delta_{II'} \tag{4.18}$$

Therefore, we obtain the trace of the density matrix

$$Tr(\hat{D}) = 1 \tag{4.19}$$

The density matrix can be used to define a mean-field one-site Hamiltonian or Fock operator.

$$F_P^{P'}(i) = H_P^{P'}(i) + \sum_j \sum_{Q,Q'} H_{PQ}^{P'Q'} D_Q^{Q'} \tag{4.20}$$

The orthonormal coefficients C_{PI} are obtained by diagonalizing the Fock operator. Hence we can define a self-consistent field procedure:

$$FC = C\epsilon \tag{4.21}$$

$$D = \frac{1}{N_I}\sum_I CC^T \quad \text{(see Eq. (4.17))} \tag{4.22}$$

$$F = H_1 + H_2 D \qquad \text{(see Eq. (4.20))} \tag{4.23}$$

This procedure in effect minimizes the mean-field energy

$$E_{SCF} = \sum_i \sum_{P,P'} H_P^{P'} D_P^{P'} + \sum_{i,j} \sum_{P,P',Q,Q'} H_{PQ}^{P'Q'} D_P^{P'} D_Q^{Q'} \tag{4.24}$$

This procedure converges for all the systems we present in the results section, and it is analogous to a Hartree Fock mean-field calculation in electronic structure theory. This calculation is the first step in the procedure and is used to obtain the exact partitioning between low-lying and high-lying states for a single site.

4.4.2 Step 2: Independent Pair Approximation for T_2 and T_s Amplitudes

For each pair of magnetic sites, we construct the pair Hamiltonian matrix.

$$M_{PQ}^{P'Q'} = H_P^{P'}\delta_Q^{Q'} + \delta_P^{P'} H_Q^{Q'} + H_{PQ}^{P'Q'} \tag{4.25}$$

Here we diagonalize the M matrix and determine $N_I * N_J$ low-lying eigenvectors C^{λ}_{PQ}, where $\lambda = 1, \cdots, N_I * N_J$. We first collect the low-lying square matrix $\tilde{C}^{\lambda}_{IJ} = C^{\lambda}_{IJ}$, and then invert this matrix to obtain S^{IJ}_{λ}. Then we can define the $\tilde{T}$-amplitudes as

$$\tilde{T}^{IJ}_{PQ} = \sum_{\lambda} C^{\lambda}_{PQ} S^{IJ}_{\lambda} \tag{4.26}$$

It can be easily verified that

$$\begin{aligned} C^{\lambda}_{PQ} &= \tilde{T}^{IJ}_{PQ} C^{\lambda}_{IJ} \\ &= \sum_{\mu,I,J} C^{\mu}_{PQ} (C^{\mu}_{IJ})^{-1} C^{\lambda}_{IJ} \end{aligned} \tag{4.27}$$

As $\tilde{T}^{IJ}_{I'J'} = \delta^{I}_{I'} \delta^{J}_{J'}$, we finally define excitation operator $\hat{T} = \tilde{T}$, except that we explicitly set all $T^{IJ}_{I'J'} = 0$. If we only consider the two-site Hamiltonian, we obtain

$$\hat{G} = (M\tilde{T})_{low-lying} = [M(1+T)]_{low-lying} \tag{4.28}$$

and it is easily verified that diagonalizing $\hat{G}$ over the low-lying states reproduces the exact low-lying eigenvalues of the full pair Hamiltonian. This method is denoted as independent pair definition of $\hat{T}$, since it is obtained by a sequence of independent pair calculations. We can obtain the pairwise G-elements in this first approximation, but the full $\hat{G}$ also contains

3- and 4-body operators. The mathematical expression can be given by

$$\hat{G} = \hat{G}_2 + \hat{G}_3 + \hat{G}_4 \tag{4.29}$$

$$= \sum_{P,Q} \hat{H}^{I'J'}_{PQ} \hat{T}^{PQ}_{IJ} + \sum_{Q} \hat{H}^{J'K'}_{QK} \hat{T}^{I'Q}_{IJ} + \sum_{R,S} \hat{H}^{K'L'}_{RS} \hat{T}^{I'S}_{IL} \hat{T}^{J'R}_{JK} \tag{4.30}$$

4.4.3 Step 3: Renormalization Transformation

Let us assume that we have obtained a suitable configurational basis, that can be partitioned into low-lying states $|I\rangle, |J\rangle, |K\rangle, |L\rangle, \cdots$ and high-lying states $|A\rangle, |B\rangle, |C\rangle, |D\rangle, \cdots$. The general states are labelled as $|P\rangle, |Q\rangle, |R\rangle, |S\rangle, \cdots$ corresponding to different sites i, j, k, l, respectively.

We also have single-site density matrices D that have elements in the low-lying range only. The only non-zero elements of D in the mean-field basis are

$$D^{I'}_{I} = \delta_{II'} \frac{1}{N_I} \tag{4.31}$$

and the density matrices are normalized. The formulae below are more general and can use any $D^{I'}_{I}$ elements, or even $D^{P'}_{P}$, using the original basis.

Let us outline the nature of the renormalization procedure first, before supplying the full details. Assume that the configurational Hamiltonian is expressed as usual as

$$\hat{H} = \sum_{i} \sum_{P,P' \in i} H^{P'}_{P} |P'\rangle\langle P| + \sum_{i<j} \sum_{P,P' \in i} \sum_{Q,Q' \in j} H^{P'Q'}_{PQ} |P'Q'\rangle\langle PQ| \tag{4.32}$$

We can write this Hamiltonian in a different fully equivalent form

$$\hat{H} = \tilde{H}_0 + \sum_i \sum_{P,P' \in i} \tilde{H}_P^{P'} |P'\rangle\langle P| + \sum_{i<j} \sum_{P,P' \in i} \sum_{Q,Q' \in j} \tilde{H}_{PQ}^{P'Q'} |P'Q'\rangle\langle PQ| \tag{4.33}$$

The new matrix elements $\tilde{H}$ satisfy the partial trace conditions

$$\sum_{P,P'} \tilde{H}_P^{P'} D_{P'}^P = 0 \tag{4.34}$$

$$\sum_{P,P'} \tilde{H}_{PQ}^{P'Q'} D_{P'}^P = 0 \tag{4.35}$$

$$\sum_{Q,Q'} \tilde{H}_{PQ}^{P'Q'} D_{Q'}^Q = 0 \tag{4.36}$$

This definition shows that it is arbitrary to some extent what one calls one-body and two-body terms. The total Hamiltonian is invariant with respect to this artificial partitioning. The above definition depends on the density matrices $D_P^{P'}$ for each site. The renormalized definitions include the state-averaged effects. Let us give a precise recipe for the renormalization.

The formulae below are defined such that the partial trace conditions in Eqs. (4.34, 4.35, 4.36) are satisfied.

$$\hat{H} = \sum_i \sum_{P,P' \in i} H_P^{P'} |P'\rangle\langle P| + \sum_{i<j} \sum_{P,P' \in i} \sum_{Q,Q' \in j} H_{PQ}^{P'Q'} |P'Q'\rangle\langle PQ| \tag{4.37}$$

For each pair of sites i and j, we obtain

$$X_{ij} = \sum_{P,P' \in i} \sum_{Q,Q' \in j} H_{PQ}^{P'Q'} D_{P'}^{P} D_{Q'}^{Q} \tag{4.38}$$

$$\bar{H}_{PQ}^{P'Q'} = H_{PQ}^{P'Q'} - X_{ij} \delta_{P}^{P'} \delta_{Q}^{Q'} \tag{4.39}$$

$$V_{P}^{P'}(j) = \sum_{Q,Q'} \bar{H}_{PQ}^{P'Q'} D_{Q'}^{Q} \tag{4.40}$$

$$V_{Q}^{Q'}(i) = \sum_{P,P'} \bar{H}_{PQ}^{P'Q'} D_{P'}^{P} \tag{4.41}$$

$$\tilde{H}_{PQ}^{P'Q'} = \bar{H}_{PQ}^{P'Q'} - V_{P}^{P'} \delta_{Q}^{Q'} - \delta_{P}^{P'} V_{Q}^{Q'} \tag{4.42}$$

Likewise for each single site, we obtain

$$X_i = \sum_{i} \sum_{P,P' \in i} H_{P}^{P'} D_{P'}^{P} \tag{4.43}$$

$$\bar{H}_{P}^{P'} = H_{P}^{P'} - X_i \delta_{P}^{P'} \tag{4.44}$$

These expressions allow us to assemble the final elements

$$\tilde{H}_0 = \sum_{i} X_i + \sum_{i<j} X_{ij} \tag{4.45}$$

$$\tilde{H}_{P}^{P'} = \bar{H}_{P}^{P'} + \sum_{j} V_{P}^{P'}(j) \tag{4.46}$$

The renormalization transformation such that partial trace are zero can be performed for any operator. Below, we will use renormalized $\hat{T}$-operators, and also renormalized $\hat{G}$

operators that can include up to four site operators. The prescription follows similar lines as for the two-body Hamiltonian discussed in detail above. Let us emphasize that the physical content of the operator is identical, e.g., diagonalizing either form of the Hamiltonian yields the same results. This has been verified explicitly in the computer code.

4.5 Definition of Effective Hamiltonian and Different Approximation Schemes

In the results section, we will consider a number of model magnetic systems that contain up to 4 magnetic sites. We will explore a number of variations of the methodology, mainly for the purpose of analyzing the importance of various effects. The model systems are chosen such that one can identify a number of low-lying states and there is a fair gap to the next higher states. Here we provide the first several steps in the calculation.

Step 1. Perform electronic structure calculation (CASSCF/CASCI) to extract the magnetic Hamiltonian parameters, as discussed in previous section 4.2.

Step 2. Identify the number of low-lying and high-lying states for each magnetic site.

Step 3. Solve the magnetic mean-field equation, and transform the Hamiltonian to the mean-field basis; renormalize the Hamiltonian to satisfy partial trace conditions. The constant term in the renormalized matrix element M is very large and is discarded as we are only interested in excitation energies at present.

Step 4. Solve the independent pair T_2 and T_s amplitudes by diagonalizing the pair Hamiltonians.

These steps are always the same, next we can introduce some different approximations.

In the first, zeroth order or bare H approach, we set T_2 and T_s amplitudes equal to zero, and hence simply diagonalize $\hat{H}$ over the low-lying configurations. In the second approach, that we label "full-T_s-pair-G_2", the $\hat{G}_2$ operator is calculated for each pair, but no 3- and 4-body effects are considered. Diagonalizing the $\hat{G}_2$ operator for a given pair exactly reproduces the pair energies of the corresponding full Hamiltonian. In the third approximation, we obtain the renormalized 1- and 2-body components of the full $\hat{G}$ operator, but we neglect the 3-body and 4-body renormalized G-elements. In addition, we employ the renormalized $\hat{T}_s$ operator that has zero partial trace, and neglect the $\hat{T}_1$ part of the renormalized $\hat{T}$-operators. These additional approximations are not needed, but they have come about for historical reasons. We plan to correct this in the near future. The important part is that this approach includes effects from the 3-body and 4-body G-elements. The approach is termed as "renorm-T_s-full-G_2". In order to compare the results from this full-G_2 approach, we also perform the pair-G_2 approach with the renormalized $\hat{T}_s$ operator, which is denoted as "renorm-T_s-pair-G_2". This will give us an idea of the importance of higher-body effects.

4.6 Results

Let us first give a brief description of the computational details. The magnetic Hamiltonians are obtained from CASSCF calculations of the state-averaged high-spin manifold using the 6-31G* basis set [67, 68] and a subsequent construction of the monomer and dimer CI matrix over the neutral configuration. Such a procedure has been implemented in the ACES II program [66]. This provides the input for the effective Hamiltonian calculations

(see section 4.2).

In analogy to chapter 3, we test the methodology for magnetic model systems that consist of an Ar atom that acts like a spacer, and this is surrounded by open-shell magnetic atoms, O, F, N and H. Oxygen atom has 9 low-lying states (^3P ground state) and 15 states in total. For F, N, and H atoms, we would simply have 6 low-lying states, 4 low-lying states and 2 low-lying states, respectively. It turns out that the effective Hamiltonian approach is extremely accurate if there is a large energy gap. For example, for NArNN magnetic system, the energy gap between low-lying and high-lying states is around 2.7 ev or 22,000 cm^{-1}.[1] In Table 4.3, we report the low-lying states energies for NArNN using the various approximations, bare H, full-T_s-pair-G_2, renorm-T_s-pair-G_2 and renorm-T_s-full-G_2 and compared to the exact energies. This system has spin symmetry, and therefore we obtain a multiplet structure. In the table, we present the energy for each magnetic level and the degeneracy of each energy level. For the renorm-T_s-full-G_2 approach, the degeneracy pattern is broken, therefore we report the *average energy* in each multiplet, and the energy spread is defined as $E_{highest} - E_{lowest}$ within a multiplet.

From Table 4.4, it can be seen that the statistical errors for each variant of effective Hamiltonian approach are extremely small. This indicates that decoupling all low-lying magnetic states from the other configurations is not a challenging benchmark for systems that have a large energy gap. This is an important result as the magnetic systems in which we are interested have this feature that the low lying magnetic states are very well separated from the high lying states. However, this does not seem to be very challenging, as even diagonalizing the bare Hamiltonian gives good results. As a result, we need to find

[1] Calculated by CASCI using the basis set of 6-31G* in ACES II package. The bond distance of Ar-N is 3.5 Å.

Level	Degeneracy	Exact	Bare H	Pair-G_2		Renorm-full-G_2	
				Full-T_s	Renorm-T_s	Avg-Energy	Spread
1	10	0.000	0.000	0.000	0.000	0.005	0.009
2	16	60.133	60.213	60.127	60.127	60.131	0.009
3	12	106.935	107.046	106.933	106.933	106.937	0.007
4	6	106.992	107.046	106.986	106.986	106.990	0.003
5	4	140.339	140.498	140.349	140.349	140.352	0.005
6	4	140.415	140.498	140.419	140.419	140.423	0.003
7	8	140.453	140.498	140.454	140.454	140.458	0.004
8	4	160.409	160.569	160.426	160.426	160.430	0.003

Table 4.3: Comparison of low-lying states energies for different approaches of NArNN. All results are in cm^{-1}.

Molecule	Statistical Errors	Bare H	Pair-G_2		Renorm-T_s-full-G_2
			Full-T_s	Renorm-T_s	
NArNN	AVG	0.086	0.006	0.006	0.007
	MAX	0.160	0.017	0.017	0.021
	RMS	0.101	0.008	0.008	0.009

Table 4.4: Statistical analysis of effective Hamiltonian data compared to exact low-lying states energies for NArNN.

more challenging systems by identifying a gap within the magnetic manifold of states and focusing the effective Hamiltonian approach on the low-lying states within the magnetic manifold. The nitrogen magnetic site is not useful as all p-orbitals in N are occupied with a single electron. However, the population of the p-orbitals in the F and O atoms is uneven and this provides interesting possibilities. The oxygen and fluorine atoms are significantly perturbed by the Ar atom. This means that the p-orbitals are not equivalent. For example, at a bond distance (Ar-F) of 2.9 Å, the spectrum for ArF is split into 2 low-lying states and 4-high-lying states with a gap of around 174 cm^{-1}.[2] Likewise, the magnetic states in ArO can be subdivided into 6 low-lying states and 3 high-lying states with a gap of about 386 cm^{-1}.[3]

In the next step, we present the geometric structures of magnetic model systems for the more challenging test.

Atom	Number of low-lying magnetic states	Number of high-lying magnetic states
O	6	3
F	2	4
H	2	0

Table 4.5: The number of low-lying and high-lying magnetic states for O, F and H atom with the inclusion of Argon atom.

[2]Calculated by CASCI using the basis set of 6-31G* in ACES II package.
[3]Calculated by CASCI using the basis set of 6-31G* in ACES II package.

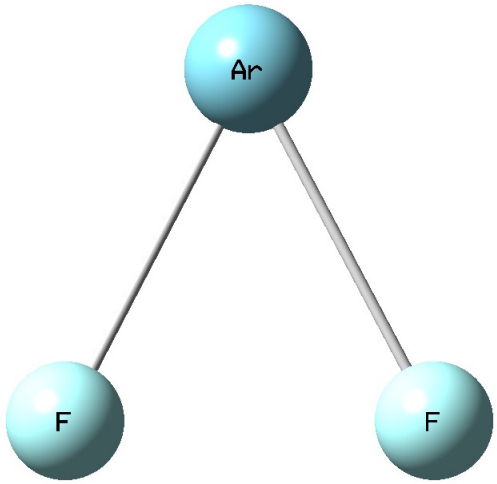

Figure 4.2: The geometric structure of FArF.

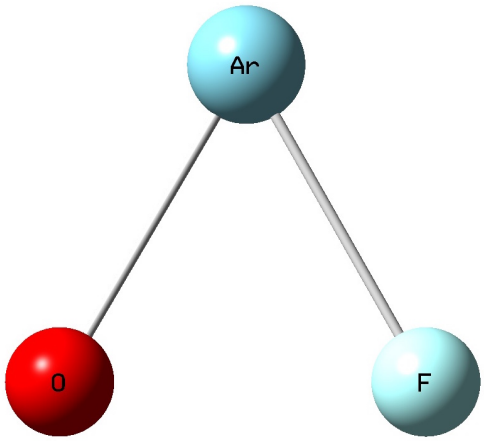

Figure 4.3: The geometric structure of FArO.

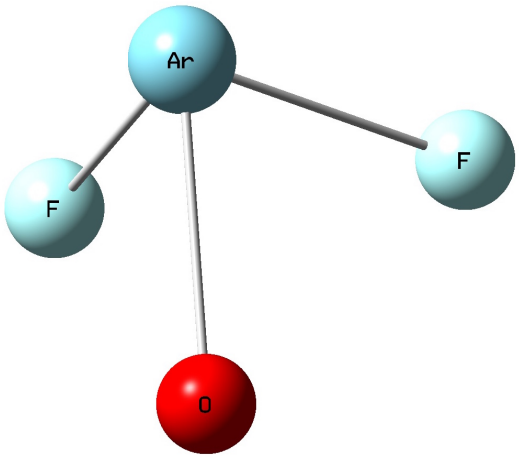

Figure 4.4: The geometric structure of FArOF.

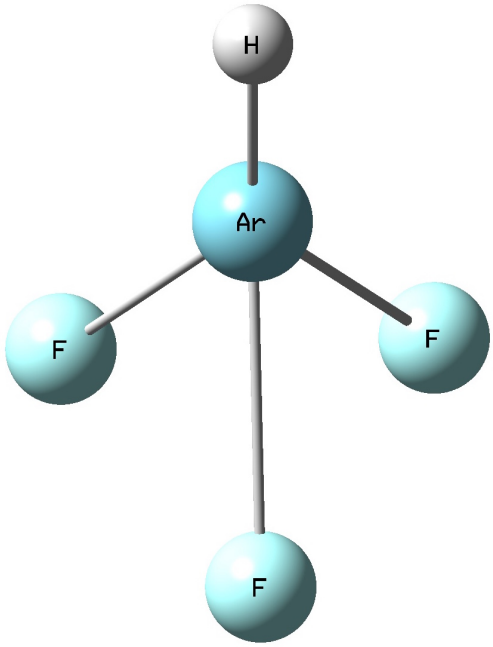

Figure 4.5: The geometric structure of HArFFF

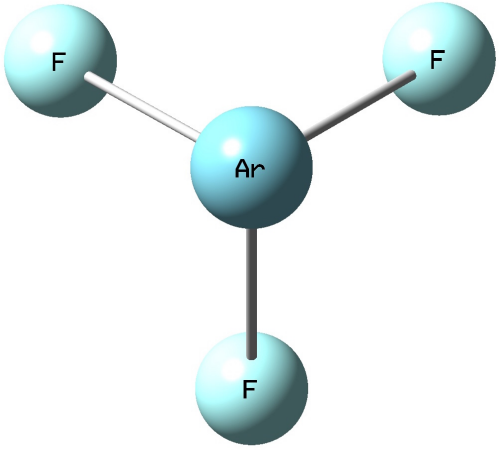

Figure 4.6: The geometric structure of FArFF

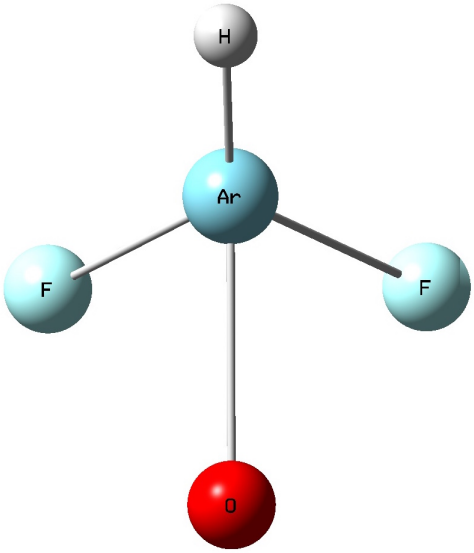

Figure 4.7: The geometric structure of HArOFF.

The specific interatomic distance of each system is given in Table 4.6.[4] For the FArOF system, we consider three slightly different structures with different interatomic distances. In addition, Table 4.6 also indicates the number of states and energy gap of each system. From Table 4.7 to 4.14, we report the degeneracies and energies of low-lying states for each magnetic system using the effective Hamiltonian approaches discussed in this work.

Molecules	Bond length (Å)				Number of States		Energy Gap (cm^{-1})	
	Ar-F	F-F	Ar-O	O-F	Total	Low-lying	Highest low-lying state	lowest high-lying state
FArF	2.586	2.800	N/A	N/A	36	4	22.891	62.281
FArFF	2.800	2.782	N/A	N/A	216	8	13.988	99.358
FArO	2.700	N/A	2.700	2.700	90	12	166.387	332.532
FArOF(a)	2.900	3.854	3.360	3.142	540	24	7.196	81.815
FArOF(b)	2.900	3.1412	2.900	3.717	540	24	11.633	79.026
FArOF(c)	2.900	3.552	2.900	3.552	540	24	8.527	95.985
HArOFF	2.900	3.552	2.900	3.552	1080	48	38.454	85.244
HArFFF	2.800	2.78170	N/A	N/A	512	16	47.894	99.437

Table 4.6: The interatomic distance, number of states and energy gap of magnetic model systems.

Level	Degeneracy	Exact	Bare H	Pair-G_2		Renorm-T_s-full-G_2	
				Full-T_s	Renorm-T_s	Avg-Energy	Spread
1	3	0.000	0.000	0.000	0.000	0.000	0.000
2	1	22.891	26.536	22.891	22.889	22.889	0.000

Table 4.7: Comparison of low-lying states energies for different approaches of FArF. All results are in cm^{-1}.

[4]The bond length of Ar-H is not presented in the table. See Appendix.

Level	Degeneracy	Exact	Bare H	Pair-G_2		Renorm-T_s-full-G_2	
				Full-T_s	Renorm-T_s	Avg-Energy	Spread
1	4	0.000	0.000	0.000	0.000	0.000	0.000
2	2	43.930	50.309	43.930	25.685	25.685	0.000
3	4	136.334	150.889	136.334	153.197	153.197	0.000
4	2	166.386	177.422	166.386	174.034	174.034	0.000

Table 4.8: Comparison of low-lying states energies for different approaches of FArO. All results are in cm^{-1}.

Level	Degeneracy	Exact	Bare H	Pair-G_2		Renorm-T_s-full-G_2	
				Full-T_s	Renorm-T_s	Avg-Energy	Spread
1	4	0.000	0.000	0.000	0.000	0.062	0.102
2	4	13.988	15.890	14.032	13.489	13.575	0.029

Table 4.9: Comparison of low-lying states energies for different approaches of FArFF.All results are in cm^{-1}.

Level	Degeneracy	Exact	Bare H	Pair-G_2		Renorm-T_s-full-G_2	
				Full-T_s	Renorm-T_s	Avg-Energy	Spread
1	5	0.000	0.000	0.000	0.000	0.196	0.368
2	6	25.476	27.744	25.798	25.196	23.440	0.063
3	3	44.322	45.088	45.023	45.030	45.248	0.161
4	2	47.894	50.288	48.309	47.711	47.979	0.004

Table 4.10: Comparison of low-lying states energies for different approaches of HArFFF. All results are in cm^{-1}.

Level	Degeneracy	Exact	Bare H	Pair-G_2		Renorm-T_s-full-G_2	
				Full-T_s	Renorm-T_s	Avg-Energy	Spread
1	6	0.000	0.000	0.000	0.000	0.008	0.019
2	6	5.550	6.773	5.656	7.368	7.449	0.038
3	4	8.551	8.739	8.623	8.306	8.315	0.014
4	4	9.057	9.403	9.305	9.148	9.156	0.014
5	4	13.853	15.213	14.033	15.464	15.547	0.029
6	4	14.864	16.114	14.918	16.484	16.564	0.040
7	2	15.974	16.290	16.102	15.620	15.630	0.015
8	2	21.025	22.451	21.253	22.558	22.645	0.017
9	2	26.780	27.205	27.102	26.941	26.950	0.007
10	2	28.667	29.233	29.094	28.781	28.791	0.005
11	2	31.946	33.302	32.095	33.480	33.748	0.012
12	4	33.020	33.511	33.496	33.654	33.490	0.011
13	2	34.144	33.542	34.339	35.768	35.856	0.019
14	4	38.453	39.802	39.651	40.363	40.455	0.027

Table 4.11: Comparison of low-lying states energies for different approaches of HArOFF. All results are in cm^{-1}.

Level	Degeneracy	Exact	Bare H	Pair-G_2		Renorm-T_s-full-G_2	
				Full-T_s	Renorm-T_s	Avg-Energy	Spread
1	5	0.000	0.000	0.000	0.000	0.012	0.022
2	5	1.552	1.811	1.497	1.877	2.033	0.001
3	3	2.321	2.347	2.355	2.000	1.873	0.001
4	3	3.454	3.346	3.383	2.723	2.725	0.001
5	3	4.361	5.024	4.403	3.933	3.960	0.001
6	3	5.380	5.992	5.424	4.784	4.817	0.007
7	1	5.761	6.066	5.785	4.137	4.137	0.000
8	1	7.196	7.785	7.257	6.155	6.188	0.000

Table 4.12: Comparison of low-lying states energies for different approaches of FArOF (a). All results are in cm^{-1}.

Level	Degeneracy	Exact	Bare H	Pair-G_2		Renorm-T_s-full-G_2	
				Full-T_s	Renorm-T_s	Avg-Energy	Spread
1	5	0.000	0.000	0.000	0.000	0.002	0.003
2	3	1.292	1.352	1.294	1.210	1.222	0.011
3	1	1.936	2.032	1.943	1.816	1.829	0.000
4	3	2.859	3.411	3.127	3.032	3.044	0.000
5	5	8.313	9.615	8.586	9.925	10.083	0.022
6	3	9.451	10.789	9.750	11.024	11.182	0.011
7	1	10.018	11.371	10.328	11.572	11.730	0.000
8	3	11.633	12.940	11.649	12.902	13.061	0.000

Table 4.13: Comparison of low-lying states energies for different approaches of FArOF (b). All results are in cm^{-1}.

Level	Degeneracy	Exact	Bare H	Pair-G_2		Renorm-T_s-full-G_2	
				Full-T_s	Renorm-T_s	Avg-Energy	Spread
1	5	0.000	0.000	0.000	0.000	0.014	0.027
2	3	1.799	1.961	1.880	1.753	1.767	0.002
3	3	2.042	2.147	2.045	1.793	1.809	0.013
4	1	3.078	3.250	3.084	2.697	2.712	0.000
5	5	5.704	6.628	5.687	6.988	7.063	0.013
6	3	7.591	8.520	7.517	8.690	8.764	0.006
7	3	7.594	8.601	7.610	8.700	8.777	0.002
8	1	8.527	9.561	8.557	9.534	9.609	0.000

Table 4.14: Comparison of low-lying states energies for different approaches of FArOF (c). All results are in cm^{-1}.

As can be seen in Table 4.7 and 4.8, the pair-G_2 approach with full T_s amplitudes reproduce the exact low-lying states energies for FArO and FArF. This is anticipated, as there is no 3-body and 4-body effects for magnetic dimers. It is of interest to note that the error of the renorm-T_s-full-G_2 approach for FArO is large. This is a consequence of the fairly small bond distance of 2.7 Å, which makes the system complicated.

Table 4.15 shows the statistical errors of these approaches compared to exact low-lying states energies for magnetic trimers and tetramers. Let us look at RMS error, which is a more straightforward look at the statistical errors. It is clear that the full-T_s-pair-G_2 approach always yields the smallest RMS for each system. This illustrates the robustness of full-T_s-pair-G_2 approach.

In addition, for the results presented above, one can see that the low-lying states ener-

gies for renorm-T_s-pair-G_2 and renorm-T_s-full-G_2 methods are close with the exception of the HArFFF system. However, the renorm-T_s-full-G_2 approach breaks the spin-symmetry. This is unexpected and is undesirable. From the analysis of the results in Table 4.15, we notice that the renorm-T_s-full-G_2 is almost always worse than the renorm-T_s-pair-G_2 approach. This is an unsatisfactory result. We anticipate that with the inclusion of 3-body and 4-body terms in the effective Hamiltonian would improve results. The fact that the spin-symmetry is broken in this approach is a clear indication that this is not a promising direction.

Molecule	Statistical Errors	Bare H	Pair-G_2		Renorm-T_s-full-G_2
			Full-T_s	Renorm-T_s	
FArFF	AVG	0.951	0.022	0.2496	0.238
	MAX	1.902	0.044	0.499	0.413
	RMS	1.345	0.031	0.353	0.295
HArFFF	AVG	1.357	0.360	0.293	0.811
	MAX	2.394	0.701	0.708	2.036
	RMS	1.693	0.438	0.390	1.119
HArOFF	AVG	0.778	0.264	0.946	1.123
	MAX	1.426	1.198	1.910	2.002
	RMS	0.924	0.394	1.200	1.270
FArOF (a)	AVG	0.542	0.028	0.647	0.680
	MAX	1.034	0.081	1.284	1.359
	RMS	0.695	0.041	0.814	0.865
FArOF (b)	AVG	0.320	0.041	0.633	0.658
	MAX	0.663	0.071	1.624	1.624
	RMS	0.408	0.046	0.791	0.798
FArOF (c)	AVG	0.751	0.147	0.798	0.877
	MAX	1.353	0.310	1.612	1.770
	RMS	0.958	0.204	1.069	1.181

Table 4.15: Statistical analysis of effective Hamiltonian data compare to exact low-lying states energies for magnetic model systems in this work. All results are in cm^{-1}

4.7 Concluding Remarks

When the work on magnetic systems was started, we had in mind to solve coupled equations for the T-amplitudes. To avoid the enormous complexity of the equations, the renormalization of amplitudes was introduced, such that partial trace were made to vanish. This approach did not turn out to be successful, and we decided to change directions. The investigation concerning the full versus renormalized T_s amplitudes in the current work was done to shed light on this aspect of the original approach. From the results presented in section 4.6, it is clear that the use of renormalized T_s amplitudes affects the results considerably and makes them worse. The inclusion of 3-body and 4-body correction to $\hat{G}_2$ (using renormalization) is relatively minor, but it breaks state degeneracy. This is very undesirable. From the present investigation, we can conclude that the independent pair approximation to define the T-amplitudes works well, but the subsequent renormalization is not a good idea.

It will also be useful to reflect on the fact that we designed systems to be quite challenging. Our initial goals were to calculate all low-lying states and to involve a decoupling only from states in which magnetic atoms were not in the ground state. This turned out to be a trivial problem since the gap is so large. Therefore, in the present calculations, we designed the systems such that due to interaction with the Ar atom, the degeneracy of the magnetic atoms was lifted and we defined an effective Hamiltonian for the subsequent low-lying states. The pair-G_2 with full T_s amplitudes approach yielded quite reasonable results and we anticipate we can improve on this by obtaining the 3-body and 4-body

contribution from the full effective Hamiltonian:

$$\hat{G} = (\hat{H}\left\{e^{\hat{T}}\right\})_{low-lying} \quad (\text{see Eq. (4.30)}) \tag{4.47}$$

This will be investigated in the near future. The method thus allows a reduction of the diagonalization space from (number of total states)$^{\text{number of site}}$ to (number of low-lying states)$^{\text{number of site}}$. This will allow us to treat larger systems, but it does not fundamentally affect the scaling. A possible solution to the diagonalization of $\hat{G}$ may be to focus on the properties of interest: free energies and magnetic susceptibilities. It may be possible to use similar ideas as presented here to make such calculation accessible. This is left to a future investigation.

The present calculations employ a model Hamiltonian without spin-orbit coupling, without dynamical correlation beyond CASSCF/CASCI, and we have neglected ionic interactions within the CAS space. In principle, all these terms will have to be included in realistic magnetic calculations. We think this can be treated mostly at the level of pairwise calculations, and we should be able to extract model magnetic Hamiltonians with the inclusion of spin-orbit coupling for preceding MREOM calculations. All of this is to be accomplished in future work.

References

[1] D. Gatteschi, R. Sessoli, and J. Villain, *Molecular nanomagnets*. OUP Oxford, 2006.

[2] J. Coey, "Magnetism in future," *J. Magn. Magn. Mater.*, vol. 226, pp. 2107–2112, 2001.

[3] J. P. Malrieu, R. Caballol, C. J. Calzado, C. De Graaf, and N. Guihery, "Magnetic interactions in molecules and highly correlated materials: Physical content, analytical derivation, and rigorous extraction of magnetic hamiltonians," *Chem. Rev.*, vol. 114, no. 1, pp. 429–492, 2013.

[4] C. Benelli and D. Gatteschi, *Introduction to Molecular Magnetism: From Transition Metals to Lanthanides*. John Wiley & Sons, 2015.

[5] E. Dagotto and T. Rice, "Surprises on the way from 1d to 2d quantum magnets: the novel ladder materials," *arXiv preprint cond-mat/9509181*, 1995.

[6] E. Coronado, F. Palacio, and J. Veciana, "Molecule-based magnetic materials," *Angewandte Chemie International Edition*, vol. 42, no. 23, pp. 2570–2572, 2003.

[7] P. A. M. Dirac, "On the theory of quantum mechanics," in *Proceedings of the Royal Society of London A: Mathematical, Physical and Engineering Sciences*, vol. 112, pp. 661–677, The Royal Society, 1926.

[8] W. Heisenberg, "Zur theorie des ferromagnetismus," *Zeitschrift für Physik*, vol. 49, no. 9-10, pp. 619–636, 1928.

[9] J. H. Van Vleck, *The theory of electric and magnetic susceptibilities*. Oxford University Press, 1932.

[10] D. Datta and M. Nooijen, "Multireference equation-of-motion coupled cluster theory," *J. Chem. Phys.*, vol. 137, no. 20, p. 204107, 2012.

[11] O. Demel, D. Datta, and M. Nooijen, "Additional global internal contraction in variations of multireference equation of motion coupled cluster theory," *J. Chem. Phys.*, vol. 138, no. 13, p. 134108, 2013.

[12] M. Nooijen, L. M. Huntington, O. Demel, D. Datta, L. Kong, K. Shamasundar, V. Lotrich, and F. Neese, "Communication: Multireference equation of motion coupled cluster: A transform and diagonalize approach to electronic structure," *J. Chem. Phys.*, vol. 140, no. 8, pp. 081102–081102, 2014.

[13] F. Neese, "Efficient and accurate approximations to the molecular spin-orbit coupling operator and their use in molecular g-tensor calculations," *J. Chem. Phys.*, vol. 122, no. 3, p. 034107, 2005.

[14] H.-J. Werner and P. J. Knowles, "An efficient internally contracted multiconfiguration–reference configuration interaction method," *J. Chem. Phys.*, vol. 89, no. 9, pp. 5803–5814, 1988.

[15] K. Shamasundar, G. Knizia, and H.-J. Werner, "A new internally contracted multi-reference configuration interaction method," *J. Chem. Phys.*, vol. 135, no. 5, p. 054101, 2011.

[16] A. Szabo and N. S. Ostlund, *Modern quantum chemistry: introduction to advanced electronic structure theory*. Courier Corporation, 1989.

[17] C. D. Sherrill, "The born-oppenheimer approximation," *School of Chemistry and Biochemistry, Georgia Institute of Technology*, 2005.

[18] I. Shavitt and R. J. Bartlett, *Many-body methods in chemistry and physics: MBPT and coupled-cluster theory*. Cambridge university press, 2009.

[19] G.-C. Wick, "The evaluation of the collision matrix," *Phys. Rev.*, vol. 80, no. 2, p. 268, 1950.

[20] T. Helgaker, W. Klopper, H. Koch, and J. Noga, "Basis-set convergence of correlated calculations on water," *J. Chem. Phys.*, vol. 106, no. 23, pp. 9639–9646, 1997.

[21] T. H. Dunning Jr, R. M. Pitzer, and S. Aung, "Near hartree-fock calculations on the ground state of the water molecule: Energies, ionization potentials, geometry, force constants, and one-electron properties," *J. Chem. Phys.*, vol. 57, no. 12, pp. 5044–5051, 1972.

[22] T. D. Crawford and H. Schaefer, "An introduction to coupled cluster theory for computational chemists," *Reviews in computational chemistry*, vol. 14, pp. 33–136, 2000.

[23] R. J. Bartlett and M. Musiał, "Coupled-cluster theory in quantum chemistry," *Rev. Mod. Phys.*, vol. 79, no. 1, p. 291, 2007.

[24] C. Bloch, "Sur la théorie des perturbations des états liés," *Nucl. Phys.*, vol. 6, pp. 329–347, 1958.

[25] J. des Cloizeaux, "Extension d'une formule de lagrange à des problèmes de valeurs propres," *Nucl. Phys.*, vol. 20, pp. 321–346, 1960.

[26] R. Maurice, R. Bastardis, C. d. Graaf, N. Suaud, T. Mallah, and N. Guihery, "Universal theoretical approach to extract anisotropic spin hamiltonians," *J. Chem. Theory Comput.*, vol. 5, no. 11, pp. 2977–2984, 2009.

[27] Z. Tabookht, X. López, C. De Graaf, N. Guihéry, N. Suaud, and N. Benamor, "Rationalization of the behavior of m2 (ch3cs2) 4i (m= ni, pt) chains at room temperature from periodic density functional theory and ab initio cluster calculations," *J. Comput. Chem.*, vol. 33, no. 21, pp. 1748–1761, 2012.

[28] C. de Graaf and R. Broer, *Magnetic Interactions in Molecules and Solids*. Switzerland: Springer, 2016.

[29] A. Ginsberg, "Magnetic exchange in transition metal complexes. 12. calculation of cluster exchange coupling constants with the x. alpha.-scattered wave method," *J. Am. Chem. Soc.*, vol. 102, no. 1, pp. 111–117, 1980.

[30] L. Noodleman, "Valence bond description of antiferromagnetic coupling in transition metal dimers," *J. Chem. Phys.*, vol. 74, no. 10, pp. 5737–5743, 1981.

[31] I. de PR Moreira and F. Illas, "A unified view of the theoretical description of magnetic coupling in molecular chemistry and solid state physics," *Phys. Chem. Chem. Phys.*, vol. 8, no. 14, pp. 1645–1659, 2006.

[32] A. Bencini, "Some considerations on the proper use of computational tools in transition metal chemistry," *Inorg. Chim. Acta.*, vol. 361, no. 14, pp. 3820–3831, 2008.

[33] A. Bencini and F. Totti, "A few comments on the application of density functional theory to the calculation of the magnetic structure of oligo-nuclear transition metal clusters," *J. Chem. Theory Comput.*, vol. 5, no. 1, pp. 144–154, 2008.

[34] F. Neese, "Prediction of molecular properties and molecular spectroscopy with density functional theory: From fundamental theory to exchange-coupling," *Coord. Chem. Rev.*, vol. 253, no. 5, pp. 526–563, 2009.

[35] A. J. Cohen, P. Mori-Sánchez, and W. Yang, "Challenges for density functional theory," *Chem. Rev.*, vol. 112, no. 1, pp. 289–320, 2011.

[36] J. Miralles, O. Castell, R. Caballol, and J.-P. Malrieu, "Specific ci calculation of energy differences: Transition energies and bond energies," *Chem. Phys.*, vol. 172, no. 1, pp. 33–43, 1993.

[37] K. Handrick, J. P. Malrieu, and O. Castell, "General strategy for the ab initio calculation of exchange coupling in polynuclear complexes," *J. Chem. Phys.*, vol. 101, no. 3, pp. 2205–2212, 1994.

[38] V. Barone, I. Cacelli, A. Ferretti, and M. Girlanda, "Toward an effective yet reliable many-body computation of magnetic couplings in bisnitronyl nitroxide biradicals," *J. Chem. Phys.*, vol. 128, no. 17, p. 174303, 2008.

[39] V. Barone, I. Cacelli, A. Ferretti, and G. Prampolini, "Modified virtual orbitals for ci calculations of energy splitting in organic diradicals," *Phys. Chem. Chem. Phys.*, vol. 11, no. 20, pp. 3854–3860, 2009.

[40] B. O. Roos, Taylor, P. R, Si, and P. EM, "A complete active space scf method (casscf) using a density matrix formulated super-ci approach," *Chem. Phys.*, vol. 48, no. 2, pp. 157–173, 1980.

[41] L. M. Huntington and M. Nooijen, "Application of multireference equation of motion coupled-cluster theory to transition metal complexes and an orbital selection scheme for the efficient calculation of excitation energies," *J. Chem. Phys.*, vol. 142, no. 19, p. 194111, 2015.

[42] L. M. Huntington, O. Demel, and M. Nooijen, "Benchmark applications of variations of multireference equation of motion coupled-cluster theory," *J. Chem. Theory Comput.*, vol. 12, no. 1, pp. 114–132, 2015.

[43] F. Neese, "The orca program system," *WIREs Comput. Mol. Sci.*, vol. 2, no. 1, pp. 73–78, 2012.

[44] H. Kramers, "L'interaction entre les atomes magnétogènes dans un cristal paramagnétique," *Physica*, vol. 1, no. 1-6, pp. 182–192, 1934.

[45] P. Anderson, "Antiferromagnetism. theory of superexchange interaction," *Phys. Rev.*, vol. 79, no. 2, p. 350, 1950.

[46] J. Kanamori, "Superexchange interaction and symmetry properties of electron orbitals," *J. Phys. Chem. Solids*, vol. 10, no. 2, pp. 87–98, 1959.

[47] H.-J. Werner, P. J. Knowles, G. Knizia, F. R. Manby, and M. Schütz, "Molpro: A general-purpose quantum chemistry program package," *WIREs Comput. Mol. Sci.*, vol. 2, no. 2, pp. 242–253, 2012.

[48] D. Mukherjee, "Normal ordering and a wick-like reduction theorem for fermions with respect to a multi-determinantal reference state," *Chem. Phys. Lett.*, vol. 274, no. 5-6, pp. 561–566, 1997.

[49] W. Kutzelnigg and D. Mukherjee, "Normal order and extended wick theorem for a multiconfiguration reference wave function," *J. Chem. Phys.*, vol. 107, no. 2, pp. 432–449, 1997.

[50] L. Kong, M. Nooijen, and D. Mukherjee, "An algebraic proof of generalized wick theorem," *J. Chem. Phys.*, vol. 132, no. 23, p. 234107, 2010.

[51] D. Datta, L. Kong, and M. Nooijen, "A state-specific partially internally contracted multireference coupled cluster approach," *J. Chem. Phys.*, vol. 134, no. 21, p. 214116, 2011.

[52] F. Neese, T. Petrenko, D. Ganyushin, and G. Olbrich, "Advanced aspects of ab initio theoretical optical spectroscopy of transition metal complexes: Multiplets, spin-

orbit coupling and resonance raman intensities," *Coord. Chem. Rev.*, vol. 251, no. 3, pp. 288–327, 2007.

[53] D. Ganyushin and F. Neese, "First-principles calculations of zero-field splitting parameters," *J. Chem. Phys.*, vol. 125, no. 2, p. 024103, 2006.

[54] B. A. Hess, C. M. Marian, U. Wahlgren, and O. Gropen, "A mean-field spin-orbit method applicable to correlated wavefunctions," *Chem. Phys. Lett.*, vol. 251, no. 5-6, pp. 365–371, 1996.

[55] Z. Liu, L. M. Huntington, and M. Nooijen, "Application of the multireference equation of motion coupled cluster method, including spin–orbit coupling, to the atomic spectra of cr, mn, fe and co," *Mol. Phys.*, vol. 113, no. 19-20, pp. 2999–3013, 2015.

[56] S. R. Langhoff and E. R. Davidson, "Configuration interaction calculations on the nitrogen molecule," *Int. J. Quantum Chem.*, vol. 8, no. 1, pp. 61–72, 1974.

[57] W. Butscher, S.-K. Shih, R. J. Buenker, and S. D. Peyerimhoff, "Configuration interaction calculations for the n2 molecule and its three lowest dissociation limits," *Chem. Phys. Lett.*, vol. 52, no. 3, pp. 457–462, 1977.

[58] T. H. Dunning Jr, "Gaussian basis sets for use in correlated molecular calculations. i. the atoms boron through neon and hydrogen," *J. Chem. Phys.*, vol. 90, no. 2, pp. 1007–1023, 1989.

[59] D. E. Woon and T. H. Dunning Jr, "Gaussian basis sets for use in correlated molecular calculations. iii. the atoms aluminum through argon," *J. Chem. Phys.*, vol. 98, no. 2, pp. 1358–1371, 1993.

[60] C. J. Calzado, C. Angeli, D. Taratiel, R. Caballol, and J.-P. Malrieu, "Analysis of the magnetic coupling in binuclear systems. iii. the role of the ligand to metal charge transfer excitations revisited," *J. Chem. Phys.*, vol. 131, no. 4, p. 044327, 2009.

[61] B. H. Brandow, "Linked-cluster expansions for the nuclear many-body problem," *Rev. Mod. Phys.*, vol. 39, no. 4, p. 771, 1967.

[62] V. Kvasnicka, "Application of diagrammatic quasidegenerate rspt in quantum molecular physics," *Adv. Chem. Phys*, vol. 36, pp. 345–412, 1977.

[63] G. Nicolas and P. Durand, "A new general methodology for deriving effective hamiltonians for atoms and molecules. application to the transferability of atomic potentials in the hydrocarbon series," *J. Chem. Phys.*, vol. 72, no. 1, pp. 453–463, 1980.

[64] C. J. Calzado, J. Cabrero, J. P. Malrieu, and R. Caballol, "Analysis of the magnetic coupling in binuclear complexes. ii. derivation of valence effective hamiltonians from ab initio ci and dft calculations," *J. Chem. Phys.*, vol. 116, no. 10, pp. 3985–4000, 2002.

[65] I. Lindgren, "Development of many-body perturbation theory," *Mol. Phys.*, vol. 108, no. 21-23, pp. 2853–2861, 2010.

[66] J. F. Stanton, J. Gauss, J. D. Watts, W. J. Lauderdale, and R. J. Bartlett, "The aces ii program system," *Int. J. Quantum Chem.*, vol. 44, no. S26, pp. 879–894, 1992.

[67] P. C. Hariharan and J. A. Pople, "The influence of polarization functions on molecular orbital hydrogenation energies," *Theor.Chim. Acta*, vol. 28, no. 3, pp. 213–222, 1973.

[68] M. M. Francl, W. J. Pietro, W. J. Hehre, J. S. Binkley, M. S. Gordon, D. J. DeFrees, and J. A. Pople, "Self-consistent molecular orbital methods. xxiii. a polarization-type basis set for second-row elements," *J. Chem. Phys.*, vol. 77, no. 7, pp. 3654–3665, 1982.

APPENDICES

Appendix A

ZMAT for Model Magnetic Systems in ACES II

A.1 NArNN

```
X
Ar 1 X
N 2 ArN 1 A
N 2 ArN 1 A 3 D
N 2 ArN 1 A 3 mD

X=1.0
ArN=3.5
A=145.0
```

```
D=120.0
mD=-120.0
```

A.2 FArF

```
F
Ar 1 ArF
F 2 ArF 1 A60

ArF=2.8
A60=55.0
```

A.3 FArO

```
F
Ar 1 ArX
O 2 ArX 1 A60

ArX=2.7
A60=60.0
```

A.4 FArFF

```
X

Ar 1 X

F 2 ArF 1 A

F 2 ArF 1 A 3 D

F 2 ArF 1 A 3 mD


X=1.0

ArF=2.8

A=145.0

D=120.0

mD=-120.00
```

A.5 FArOF (a)

```
X

Ar 1 X

O 2 ArO 1 A

F 2 ArF 1 A2 3 D

F 2 ArF 1 A2 3 mD


X=1.0
```

```
ArO=2.9

ArF=2.9

A=135.0

A2=135.0

D=110.0

mD=-110.0
```

A.6 FArOF (b)

```
X

Ar 1 X

O 2 ArO 1 A

F 2 ArF 1 A2 3 D

F 2 ArF 1 A2 3 mD


X=1.0

ArO=2.9

ArF=2.9

A=135.0

A2=135.0

D=130.0

mD=-130.0
```

A.7 FArOF (c)

```
X
Ar 1 X
O 2 ArO 1 A
F 2 ArF 1 A2 3 D
F 2 ArF 1 A2 3 mD

X=1.0
ArO=2.9
ArF=2.9
A=135.0
A2=135.0
D=120.0
mD=-120.0
```

A.8 HArOFF

```
H
Ar 1 ArH
O 2 ArO 1 A
F 2 ArF 1 A2 3 D
F 2 ArF 1 A2 3 mD
```

```
ArH=2.0

ArO=2.9

ArF=2.9

A=135.0

A2=135.0

D=120.0

mD=-120.0
```

A.9 HArFFF

```
H

Ar 1 X

F 2 ArF 1 A

F 2 ArF 1 A 3 D

F 2 ArF 1 A 3 mD


X=2.0

ArF=2.8

A=145.0

D=120.0

mD=-120.0
```